Geomorphology
April 2022, Volume 402, Pages 108133 (18p.)
https://doi.org/10.1016/j.geomorph.2022.108133
https://archimer.ifremer.fr/doc/00750/86174/

Common origin of coexisting sediment undulations and gullies? Insights from two modern Mediterranean prodeltas (southern Italy and northern Morocco)

Clementucci R. [1, 2, 5, *], Lafosse M. [3, 6], Casalbore D. [4, 5], Ridente D. [4], D'Acremont E. [6], Rabaute A. [6], Chiocci F.L. [5], Gorini C. [6]

[1] Dipartimento di Scienze, Università Roma Tre, Italy
[2] Aix-Marseille Univ., CNRS, IRD, INRAE, Coll. France, CEREGE, Aix-en-Provence, France
[3] Department of Earth Sciences, Utrecht University, Netherlands
[4] Istituto di Geologia Ambientale e Geoingeneria (CNR), Sede Sapienza Università di Roma, Italy
[5] Dipartimento di Scienze della Terra, Università Sapienza di Roma, Italy
[6] Sorbonne Université, CNRS-INSU, Institut des Sciences de la Terre Paris, ISTeP UMR 7193, Paris, France

* Corresponding author : R. Clementucci, email address : romano.clementucci@uniroma3.it

Abstract :

Depositional and erosional bedforms that shape prodelta deposits in the Gulf of Patti (southern Tyrrhenian Sea) and in the Al-Hoceima Bay (northern Morocco) were investigated using multibeam bathymetry as a basis for morphometric analysis. The two study areas have comparable structural settings and oceanographic regimes and share the occurrence of sediment undulations and closely spaced gullies. The resulting bedform fields are confined on prodelta deposits, from the inner to the outer shelf. The infrequent coexistence of these two types of bedforms on other Mediterranean margins makes our case study an ideal opportunity to investigate the processes that may control the combined or independent genesis of each type of bedform. Whereas gullies are more confidently interpreted as the result of erosion of the seafloor by hyperpycnal flows generated at river mouths and/or triggered by settling plumes and small-scale instabilities on delta front, unveiling the genetic mechanism behind sediment undulations is more difficult, and makes identifying the underlying processes, ranging from bottom currents to gravity flows or even internal waves, more ambiguous. Quantitative measurements of the main morphometric parameters of sediment undulations and gullies were computed to resolve relationships between their variability and their distribution over the prodelta area. Particular attention was paid to statistical analysis of sediment undulations using multivariate analysis based on principal component analysis (PCA) and k-mean fuzzy clustering. The individual and comparative analyses suggest that shelf gradients, location and distance from the river mouth, and sediment supply are keys in controlling the growth and scale of sediment undulations with respect to their distribution downslope. Although from our analysis, sedimentary gravity flows stand out as the most likely mechanism triggering the generation of sediment undulations, alternative causes (i.e., soft-sediment deformation or sediment remobilization by oceanographic processes) cannot be ruled out. Our results provide new insights into the possible origin of sediment undulations under the control of river-driven sediment gravity flows in prodelta settings, indicating that their concomitant occurrence with gullies is not accidental.

Highlights

► Genesis of coexisting depositional and erosional bedforms in prodelta settings ► Quantitative and statistical analysis to unveil the mechanism behind the bedforms ► Controlling factors of the sedimentary gravity flows and associated bedforms

Keywords : Sediment gravity flows, Quantitative geomorphology, Gullies Sediment undulations, Mediterranean prodeltas

1. Introduction

High-resolution morpho-bathymetric and seismic-stratigraphic analyses that have been extensively performed on modern prodelta systems, have revealed the occurrence of widespread erosional and depositional bedforms, typically consisting of sediment undulations and gullies, respectively (e.g., Urgeles et al., 2011). Sediment undulations in prodelta deposits on shallow shelf settings usually top Late-Holocene Highstand Systems Tract (HST), and are seismically imaged as a wavy geometry of clinoform reflectors (Correggiari et al., 2001; Urgeles et al., 2007, 2011; Casalbore et al., 2017).

Sediment undulations on prodelta deposits commonly extend between 20 and 120 m water depths (wd, hereafter), with crest elongation roughly parallel to the bathymetric contours. Their scale varies considerably, with wave heights ranging from a few centimeters to 5 m, wavelengths up to 300 m, and lateral extensions up to several kilometers (Urgeles et al., 2011). In cross section, the undulations usually display landward asymmetry with shorter upslope limbs. Gullies are seafloor incisions hundreds of meters long, a few meters to tens of meters wide, and a few meters deep, typically located on shelf and slope sectors in front of river mouths (Flood, 1981; Chiocci and Normark, 1992; Field et al., 1999; Maillet et al., 2006; Chiocci and Casalbore, 2011; Lobo et al., 2014).

Whereas gullies have been confidently linked to river processes, such as the plunging of hyperpycnal flows directly from the river mouth and/ or triggered by settling process from river plume (Hill, 2012; Lintern et al 2016; Hizzett et al., 2018; Hage et al., 2019; Hill and Lintern 2021), the processes linked to the origin of sediment undulations are the subject of lively debate. In particular, sediment undulations of overall similar scale and shape have been alternatively interpreted as (i) in-situ deformation of soft sediment, known as creep (Ercilla et al. 1995; Belotti et al., 1994; Correggiari et al., 2001; Lykousis et al., 2009, Li et al., 2016),

a process commonly favored by high sedimentation rates (Duchesne et al., 2003) or by liquefaction along a weak basal layer induced by dynamic loading, for instance during earthquakes (Berndt et al., 2006; Sultan et al., 2008); (ii) sediment transport and deposition during energetic processes, such as hyperpycnal flows (Urgeles et al., 2007; Fernández-Salas et al., 2007; Lobo et al., 2015); (iii) sediment remobilization by water mass dynamics, such as bottom currents (Correggiari et al., 2001; Cattaneo et al., 2003) and internal waves (Puig et al., 2007; Van Haren and Puig, 2017; Li et al., 2019).

Bearing these uncertainties in mind, here, we focus on the genesis of the sediment undulations on two Mediterranean prodeltas (Fig. 1): the Mazzarrà prodelta in the Gulf of Patti (southern Italy, Tyrrhenian Sea), and the Rhis-Nekor prodelta in Al-Hoceima Bay (northern Morocco, Alboran Sea). In both prodeltas, the sediment undulations are cross cut by arrays of gullies, reflecting the importance of riverine activity in eroding the seafloor and, perhaps, also in shaping the sediments (Casalbore et al., 2017; Lafosse et al., 2018). The coexistence of these different bedforms in our two study areas provides an opportunity to investigate possible linkages between the generation of sediment undulations and gullies, which would allow us to infer a common origin controlled mainly by sediment gravity flows related to river activity and/or in minor contribution by oceanographic processes, such as internal waves. We conducted a detailed morphometric and geostatistical analysis of their main geometric and dimensional features based on the more problematic nature of sediment undulations, in order to: (a) define variability patterns of morphometric parameters in each area; (b) compare variability patterns in the two areas to identify similarities and differences; (c) define any possible cause-effect relationship between similarities/differences emerging from the above comparison and the specific features that distinguish the two shelf environments.

Our results indicate that the recurrence and energy of sedimentary gravity flows and hence the development of the associated bedforms are mainly linked to the variation of the slope gradient, shelf morphology and river supply dynamics. More generally, this paper highlights the critical role of studying and comparing the coexistence of different geomorphic features and provides insights that can serve similar comparative analyses of prodeltas located on other margins.

2. Geological background

2.1 Gulf of Patti

The Mazzarrà prodelta is located in the Gulf of Patti (NE Sicily), along the southern Tyrrhenian margin (Fig. 1a). The Gulf of Patti is on the northern margin of the Peloritani Mountains, the southernmost part of the Calabria-Peloritani Arc. This arc is an allochthonous crustal block where the Kabilo-Calabride units thrust over the Apennine units (Lentini et al., 1996; Lentini et al., 2006). The crystalline basement is unconformably overlain by Mesozoic limestones and Cenozoic flysch deposits (Lentini et al., 2006). After compressive phase thrusting, the continental margin in this sector experienced post-collisional extensional tectonics associated with the southern Tyrrhenian rifting and back-arc basin formation (Faccenna et al., 2001; Cuffaro et al., 2011). As a result, two major right-stepping faults: the Tindari-Rocca Novara Fault zone (TNFZ) to the south, and the Vulcano-Milazzo fault zone (VMFZ) to the north (Cultrera et al., 2016, Fig. 1a) bound the Gulf of Patti. Instrumental seismicity in the study area is significant, with more than 2,000 events of between Mw 1.0 ≤ and Mw ≤ 4.8 in the last 30 years with strongest events reaching Mw ~ 6 (Chiarabba et al., 2005; Cultrera et al., 2016).

The coastal and mountainous sectors of the Peloritani are affected by tectonic uplift (Westaway et al., 1993), at rates estimated in the order of 1 mm/yr in the last 125 ky (Ferranti et al., 2010). Consequently, short watercourses forming relatively small drainage basins with high slope gradients and torrential regimes characterize the regional hydrographic setting. These small, intermittently active rivers are locally named "Fiumara" and are known for the occurrence of extreme flash-flood events (Sabato and Tropeano, 2004).

The Mazzarrà River has a fiumara type course about 24 km long, with a drainage basin of about 120 km^2. The source area rises to 1200 m above sea level, with an average slope gradient of 4.9° (up to 6° in the upper part) that rapidly decreases towards the coastal plain (Table 1). Based on hydrological data, the maximum discharge of the Mazzarrà River is estimated between 500 and 777 m^3/s, with a recurrence time for intense flash-floods of 50 and 300 years (http://www.sitr.regione.sicilia.it/pai/bacini.htm). During flash-floods, small landslides and debris flows occur on the valley flanks and the Mazzarrà River increases its sediment transport capacity, thereby ensuring a large supply of sediment to the coast (Sabato and Tropeano, 2004; Casalbore et al., 2017). This sediment sources a shelf sector with a low tidal excursion (maximum 0.6 m;

Istituto Idrografico della Marina, 1982), where the seasonal wind-driven wave regime produces storm waves up to 3–4 m in height. Finally, sourcing dynamics have been affected by anthropic activities, causing the river mouth to switch eastward, possibly after the 1960s (Casalbore et al., 2017). Here, two main types of sediment undulations have been described on the prodelta area, based on their location and morphology: unconfinated undulations () and channel confined undulations (Type A and B, respectively from Casalbore et al., 2017).

2.2 Al-Hoceima Bay

Al-Hoceima Bay (NE Morocco) in the southern Alboran Sea, is fed by the Rhis and Nekor Rivers (Fig. 1b), which form two amalgamated prodelta deposits hereafter referred to as the Rhis-Nekor prodelta. The two rivers and the shelf where the prodelta develops are part of a margin sector bounded by the Rif mountain belt (Fig. 1b), which, like other Mediterranean orogens, was emplaced during the Eocene-Oligocene tectonic phase due to Africa and Eurasia convergence and later affected by a back-arc extension (Chalouan et al., 2008). The crustal basement of the chain belt is structured in southwest-verging nappes (Wildi, 1983), whereas Al-Hoceima Bay is located within the transensional structure called the Nekor Basin formed during the Quaternary (Calvert et al., 1997; Lafosse et al., 2017, Tendero-Salmerón et al., 2021), the most seismically active sector in the Alboran Basin (El Alami et al., 1998; Stich et al. 2005; Stich et al., 2020).

The Nekor Basin is bounded by the left-lateral Boussekkour-Aghbal and Bokkoya faults to the north (d'Acremont et al., 2014; Lafosse et al., 2017), and by the normal-sinistral Trougout fault to the east (Fig. 1b). Based on U-Th dating of raised marine terraces, the Rif belt has been affected by an uplift rate of 0.2 mm/yr since the Upper Pleistocene (Morel and Meghraoui, 1996; Poujol et al., 2014). Based on the kinematic and uplift rate of the Trougout fault in Ras Tarf, at least 0.5 mm/yr of subsidence of Al-Hoceima Bay can be hypothesized (Fig. 1b) (Poujol et al., 2014).

The rivers draining the Rif belt form the typical networks of tectonically active regions in a semi-arid climate, characterized by accelerated incision and steep river courses in response to the regional uplift (Barcos et al., 2014). The Nekor River watercourse is 82 km long and is supplied by a drainage basin that can reach 854 km^2 in width, with a maximum elevation of 1300 m above sea level (asl). The Rhis River is 78 km long, with a drainage basin 836 km^2 in width and maximum elevation of 1180 m asl. (Table 1). The average slope gradient of the Nekor and Rhis River drainage basins is ~1.5°, and reaches maximum values of

2° in the upper course. Minimum values of less than 1° are measured in the alluvial plain, which is 12 km wide and covers an area of 92 km^2.

The prevailing lithotypes in the drainage basin consist of schists, limestones, and marly limestones from the Cretaceous Ketama unit, with a smaller proportion of metamorphic rocks located in the western Nekor Basin (Amil, 1992). The average maximum rainfall occurs in winter reaching 340 mm/yr (Amil, 1992), providing enough water for sudden flash-floods (Abdalla et al., 2014); the an annual river discharge is 2.17 m^3/s (Table 1). However, water and sediment fluxes are hampered by the Al-Khattabi dam, built on the Nekor River in 1981 (Chafouq et al., 2018).

The Al-Hociema Bay is characterized by a wide shelf with low gradients (less than 1.5° on average), characterized by an extensive surface identified as submarine terraces (Lafosse et al., 2018). The shelf is highly exposed to current perturbation induced by internal waves and storm events with waves up to 5 m high with dominant WNW wave direction (Khouakhi et al., 2013; Ercilla et al., 2016).

The oceanographic circulation in the Alboran Sea is the result of the input and mixing of Atlantic water with the western Mediterranean deep water masses, forming a quasi-permanent anticyclonic gyre with east to west sedimentary transport (Viúdez et al., 1998; Juan et al., 2016; Ercilla et al., 2016). The circulation pattern likely influences the shelf area of Al-Hoceima Bay (Gascard and Richez, 1985), where the studied prodelta deposits are also located.

3. Data and methods

3.1 Geophysical dataset

Extensive multibeam morpho-bathymetry and more limited high-resolution seismic data were collected in the Gulf of Patti between 2010 and 2016, aboard the R/V Urania and Minerva-Uno Research Vessels of the National Research Council (CNR). The area covered by multibeam data is ~75 km^2, at depths ranging between 20 and 1000 m (Fig. 3a). Data were acquired using a Kongsberg EM710 multibeam system (70-100 kHz) and DGPS-positioning and processed using Caris HIPS and SIPS. The generated digital elevation models (DEMs) have a variable cell size, from 1 m in shallow water to 20 m in deeper water. The high-resolution seismic profiles were acquired using a Teledyne BENTHOS III CHIRP system (2-20 kHz) along a grid with average 300 m line spacing. Seismic data with a vertical resolution of 0.5 m were processed using

GeoSuite software for automatic gain control (AGC) and time variable gain (TVG); IHS Kingdom software was used for the interpretation and correlation of key seismic reflectors and units.

Multibeam bathymetric data and high-resolution seismic profiles in the Al-Hoceima Bay were collected during two oceanographic surveys in 2012: the Marlboro-2 and the SARAS surveys (Fig 3b) (d'Acremont et al., 2014). Multibeam data were acquired using a shallow-water Reson 8101 system during the MARLBORO-2 survey and an Kongsberg EM710 system during the SARAS survey. QUINCY and CARAIBES (IFREMER) software were used to process data and generate DEMs; both have a cell size of 5 m and vertical resolution of 0.5 m for water depths below 100 m (MARLBORO-2 survey). The 2D seismic profiles were acquired using a 250–500 J SPARKER source and a six channel streamer. High-resolution parametric profiles (TOPAS PS18, 15 –21 kHz, 32kW) were also acquired during the SARAS survey. The seismic data were stacked, filtered and migrated using SEISMIC UNIX software and imported into IHS Kingdom software for seismic interpretation.

3.2 Quantitative and statistical analysis

To study the genetic mechanisms of similar bedforms in the two study areas requires defining the sedimentary background in terms of sediment sourcing to the shelf and undertaking quantitive analysis of relevant morphometric parameters. One main factor controlling seafloor geomorphic shaping is the amount of sediment delivered to the shelf and slope (Casalbore et al., 2011; Gamberi et al., 2014). It is thus important to define how drainage basin settings can influence the sediment load and yield. These were estimated by applying the equations of Milliman and Syvitski (1992), based on the relationship between the elevation of the drainage basin area, sediment load, sediment yields, and the geographical region (see supplementary material, Appendix SM1).

To define morphological patterns in displaying sediment undulations in both the study areas, each bedform was detected and defined as a trough-crest-trough triplet (Figs. 2c, 2d). The next step consisted of the automatic computation of relevant morphometric parameters derived from each trough-crest-trough triplet (see supplementary material**,** Appendix SM2). These include (Fig. 2e): wave height (*H*), wavelength (*L*), lateral length (*Ll*), basal slope (*S*), and asymmetry (*Asym*). A principal component analysis (PCA; see supplementary material, Appendix SM3) was performed on four of these morphometric parameters (*H, L, H/L, Ll*), combined with their corresponding water depth, distance from the river mouth and slope gradient.

PCA is useful to estimate the relative importance of the different morphometric parameters in explaining the variability of the bedforms on the seafloor (Symons et al., 2016). We also took the thickness of a stratigraphic interval corresponding to the Late Holocene high stand system tract (HST; Casalbore et al., 2017; Lafosse et al., 2018) into account because this paramenter varies linearly with water depth and distance from the coastline and hence allowed us to crosscheck the consistency of other parameters that are also assumed to vary with water depth and distance from the coast.

Finally, the results of the PCA were used to identify eight clusters of spatially coherent populations (see supplementary material, Appendix SM4). The clusters are plotted in map view to highlight the spatial characterization of the bedforms. To quantitatively estimate the difference between the two areas, the clustering indexes were tested against the variables and the results are reported in boxplots.

4. Results

4.1 Gulf of Patti

4.1.1 The Mazzarrà prodelta

The Mazzarrà prodelta covers 15 km^2 of the surveyed area, encompassing a shelf sector between 30 and 120 m water depths (wd, hereafter). The seafloor in this area is characterized by sediment undulations and superposed gullies between 35 m wd and the shelf edge (Fig. 3a, 3c). The undulations show sinuous crests in the plan-view and an overall irregular shape, locally reflecting the superposition of smaller undulations over larger ones (Fig. S3 in supplementary materials). Overall, the crests are parallel or sub-parallel to the bathymetric contour, with a main NE-SW trend near the river mouth, and an E-W orientation in deeper water (Figs. 3a, 3c, and 4a). The bulk of the prodelta deposits are part of a low-angle prograding HST, previously defined based on the geometry of seismic reflectors (Casalbore et al., 2017). These show an undulating pattern that mimics the sediment undulations on the seafloor, indicating several generations of bedforms separated by thinner, seismically transparent intervals (Fig. 5a). The boundary between the HST and the underlying transgressive systems tract (TST) is roughly marked by the transition from undulating seismic reflectors to regular and progressively flatter reflectors, indicating the progressive attenuation of the low-angle progradational geometry (mfs; Fig. 5a). The base of the TST is a marked erosional unconformity; like on other Quaternary margins, it is a polygenic erosional surface recording sub-aerial exposure during the last

glacial sea-level fall and lowstand, followed by marine ravinement erosion during the subsequent post-glacial sea-level rise (Lobo and Ridente, 2014, Ridente, 2016). The HST unit as defined above reaches a maximum thickness of 25-30 m close to the river mouth, and then thins seaward into a distal drape locally eroded, although more frequently extending to the shelf edge and upper slope (Fig. 5a).

4.1.2 Gullies and sediment undulations on the Mazzarrà prodelta

A total of 75 shelf gullies have been mapped in the Mazzarrà prodelta, 36 of which incise the shelf edge (Table S1 in supplementary material). These differ in presenting a V- or U-shaped thalweg in cross section. This morphological distinction correlates with the overall distribution since U-shaped gullies are preferentially located between 30 and 50 m wd (red lines in Fig. 3c), whereas V-shaped gullies occur in deeper water. U-shaped gullies are up to 300 m long, 100 m wide and incise the seafloor to a depth of 1 m near the abandoned western branch of the Mazzarrà River (red lines in Fig. 3c). Figure 3c shows Channel A (ChA), the largest U-shaped gully on the shelf. The gully is ~1 000 m long, 100 m wide, and 3 m deep. Upslope, it connects with the front of the present-day mouth of the Mazzarrà River. Downslope of Channel A, a network of V-shaped gullies ranges between 40 and 120 m wd. They are between 280 and 2400 m long and between 30 m and 240 m wide, the incision depth ranges between 0.1 and 3.5 m (Table S1). Their spatial distribution is radial with respect to both the present-day and nearby abandoned branches. Their incision depth generally decreases downslope (Fig. S4 in supplementary material). The gullies cutting the shelf edge also are V-shaped. On average, they are 500 m long, 80 m wide, and incise the seafloor to a depth of 6 m (Table S1). To the west, near the mouth of the Elicona Fiumara, smaller gullies are present at a distance of 1-2 km outside the undulation field, converging towards an area of irregular seafloor spotted by bedrock relief (Figs. 3a, 3c).

A total of 596 individual sediment undulations were mapped in the Mazzarrà prodelta area (including both Type A and B); wave heights (*H*) range between 0.05 and 4.4 m (yielding an average of 0.77 m; Table 2). The higher *H* values are concentrated between 45 and 100 m wd in two sectors of the prodelta facing the abandoned and present-day river mouths (Fig. 6a), while *H* values decrease landward at depths shallower than 45 m, reaching a minimum of 0.1 m; these lower values are comparable with those measured on the outer shelf (beyond 100 m wd) and in the western part of the prodelta area (Fig. 6a). The wavelengths (*L*) of

the undulations range between 16 and 242 m (average value 74 m; Table 2), and their spatial distribution displays no pattern with respect to depth or distance from the river mouth (Fig. 6b).

The aspect ratio (*H/L*) of the undulations varies between 0.001 and 0.032 (average value 0.007; Table 2), with the highest values (~0.03) occurring at water depths greater than 45 m in the areas facing the present-day and abandoned river mouths (Fig. 6c). The *H/L* ratio shows even clearer spatial bipartition than that of *H*. Outside these two areas, *H/L* spans between 0.01 and 0.016 (Fig. 6c). Asymmetry (*Asym*) ranges between 0.81 and 0.62 (average value -0.007; Table 2), with positive values prevailing and overall uniform spatial distribution. The negative values are more scattered, though they tend to concentrate in front of channel A, where the undulations have higher *H* and *H/L* (Figs. 6a, 6c, 6d).

The lateral length (*Ll*) values yield a minimum of 30 m and a maximum of 1,310 m (average 220 m; Table 2), with higher values locally concentrated in two depth ranges, one between 50 and 70 m wd, and the other between 80 and 120 m wd; values then decrease significantly in front of the river mouth (Fig. 6e). The basal slope of the undulations (*S*) ranges between 0.46° and 2.75° (average value 1.4°; Table 2), with the highest values on the inner and middle shelf, then progressively decreasing to 0.80° towards the shelf edge (Fig. 6f).

4.2 Al Hoceima Bay

4.2.1 The Rhis-Nekor prodelta

The Rhis-Nekor prodelta lies on a 6 km wide continental shelf with relatively uniform gradients (generally less than 1.0°; Fig. 4b), except for a marked submarine terrace (Lafosse et al., 2018) that extends 6 km SW-NE at around 80 m wd and forms a seafloor scarp up to a height of 5 m (Figs. 3d and 4b). The scarp is partly buried below the prodelta deposits with lateral elongation roughly parallel to the isobaths (Fig. 3d). The prodelta deposits cover an area of approximately 30 km^2, extending at depths between 30 (landward limit of the bathymetric survey) and 100 m (Figs. 3b, 3d). Overall, the shelf edge is regular and occurs at depths of between 100 and 110 m, where seafloor gradients increase to values of 2° (Fig. 4b).

The prodelta can be divided into two morphological sectors that basically reflect the composite nature of the source, consisting of the mouths of the Rhis and Nekor Rivers located 4 km apart along the coastline (Figs. 1b and 3d). The prodelta sector on the side of the Nekor River mouth (light blue patch in Fig. 3d) has a slightly convex-seaward shape in plan-view and is characterized by gullies and sediment undulations

developing at 30 m wd (this is the limit of the bathymetric survey). The prodelta sector in front of the Rhis River mouth (brown patch in Fig. 3d) has a very subtle seafloor expression and is characterized by gullies and undulations originating at 35 m wd. In both sectors, sediment undulations exhibit roughly linear crest lines (Figs. 3d and 4b), generally elongated parallel to the bathymetric contours.

Similarly to the southern Tyrrhenian margin, the prodelta deposits are at the top of the post-glacial TST-HST succession recording the Late Pleistocene-Holocene transgression and Late Holocene highstand (Fig. 5b). The thickness distribution of the HST was defined by Lafosse et al. (2018) and shows the main depocenter near the mouths of the Rhis and Nekor Rivers, with an overall uniform thickness of ~20 m (locally reaching 25 m) between 30 and 60 m wd; the lateral variability of depocenters is more pronounced between 60 and 90 m wd (maximum values of ~10 m), then rapidly decreases towards the shelf edge as the HST thins out (Fig. 4d).

4.2.2 Gullies and sediment undulations on the Rhis-Nekor prodelta

A total of 83 V-shaped shelf gullies were mapped in the Rhis-Nekor prodelta (Table S2 in supplementary material). The lengths of the gullies range from 190 to 3000 m, cutting through the sediment undulations (Figs. 3b, 3d). Their widths and incision depths range from 10 to over 200 m and from 0.1 to 1.7 m, respectively (Table S2). In the prodelta sector closer to the Rhis River mouth, the flow direction of gullies converge slightly on the inner shelf and become linearly spaced on the middle and outer shelf. In contrast, on the prodelta side in front of the Nekor River mouth, the gullies have an overall straight trend and are regularly spaced (Figs. 3b, 3d). Overall, their incision depth and width reach maximum mid-shelf (around 50-70 m wd) and decrease seaward (Fig. S5 in supplementary material). To the west and away from the Rhis-Nekor main sediment entry points, the sediment undulations fade out and only a few shallower gullies occur between 65 and 90 m wd (Figs. 3b, 3d).

We measured 510 sediment undulations in the Rhis-Nekor prodelta; their wave height (*H*) ranges from 0.04 to 2.33 m (average 0.8 m; Table 2), with greater *H* values at depths between 60 and 95 m wd in front of the Rhis River mouth. Here, the sediment undulations are well-developed downslope of the submarine terrace. The *H* values decrease significantly towards the river mouth and nearby areas, for instance above the submarine terrace and close to the shelf edge (Fig. 7a). The wavelength (*L*) of the undulations varies between

40 and 456 m (average 142 m; Table 2), the higher values are concentrated in the prodelta sector close to the Rhis River mouth, although scattered high values also occur in the Nekor prodelta sector (Fig. 7b). Overall, *L* values display similar distribution to *H* values.

The aspect ratio (*H/L*) varies between 0.001 and 0.015 (average value 0.004; Table 2), with less variability than undulations in the Mazzara prodelta (Fig. 7c). Asymmetry (*Asym*) varies between -0.73 and 0.68 (average 0.008; Table 2), with predominantly positive values indicating slight asymmetry upslope. The lateral length (*Ll*) ranges between 22 and 3043 m (average 312 m; Table 2). The greater lateral lengths occur between 65 and 95 m wd (Fig. 7e) along the buried submarine terrace (similarly to the *H* and *L* distribution); *Ll* values also increase off the mouth of the Nekor River. The basal slope of the undulations (*S*) ranges from 0.11 to 1.99°, with an average of 0.86° (Table 2). The highest values are found in the prodelta sector close to the Rhis River mouth, whereas they decrease seaward and laterally towards the Nekor River mouth (Fig. 7f).

4.3 Principal component analysis of the sediment undulations

In order to distinguish morphological patterns, sediment undulations in each study area were investigated using principal component analysis (PCA) and fuzzy c-mean clustering, performed on the morphometric parameters (*H, L, H/L, Asym*) and background environmental factors (water depth, basal slope, distance from the river mouth, HST thickness). The first four principal components (referred to as PC1-PC4 in Table 3) explain 86% of total variability whereas the other principal components (PC5-PC8 in Table 3) account for the remaining 14% of variance in the dataset.

PC1 and PC2 are correlated with *H, L*, and *S*, as well as with the distance from the river mouth and, consequently, with the thickness of the HST (Table 3). PC3 and PC4 are correlated with *Asym* and water depth (Table 3). PCA defined eight clusters within the global variability space (Fig. 8, supplementary materials Fig. S2); boxplots show the different distribution of the parameters measured for each cluster (Fig. 8).

Sediment undulations in the Mazzarrà prodelta are represented by clusters 1, 2, and 3 (Fig. 8a; pink area in the boxplot in Fig. 9), indicating an approximately linear variation with water depth and distance from the river mouth (Figs. 9a, 9c; paralleled by the variation in thickness of HST in the prodelta area). The basal slope of the undulations showed no clear trend (Fig. 9g), but cluster 3 showed significantly lower values than

clusters 1 and 2 (Fig. 9g). Cluster 2 (green points in Fig. 8a) is prevalent off the abandoned and present-day river mouth. Regarding the morphometric parameters, cluster 2 shows higher *H* and *H/L*, slightly higher *L* values, and slightly negative *Asym* values compared to clusters 1 and 3 (pink boxplot in Figs. 9b, 9d, 9f, 9h).

Sediment undulations in the Rhis-Nekor prodelta are represented by clusters 4-5-6-7-8 (Fig. 8b; blue field in the boxplot in Fig. 9), indicating approximately linear variation with distance from the river mouth and water depth (Figs 9a, 9c) whereas a more complex pattern is shown by *S* and HST thickness (Figs. 9e, 9g). In particular, clusters 4 and 5 are located closer to the river mouths (less than 4.5 km away, landward of the 70 m isobath). Cluster 6 is mainly located above the submarine terrace, where *S* and HST thickness both decrease significantly (Fig. 8b; blue field in the boxplot in Figs. 9e, 9g). Cluster 7 is oriented obliquely along the prodelta area, downslope of the submarine terrace. Cluster 8 is located on the outer shelf, mainly in the westernmost part of the prodelta, where *S* and HST thickness decrease dramatically (Fig. 8b; blue field in the boxplot in Figs. 9e, 9g).

Regarding the morphometric parameters, clusters 5 and 7 show markedly higher *H* and *L* values than the other clusters (blue area in Figs. 9b, 9d). In contrast, there are only minor differences between the *H/L* clusters (Fig. 9f) due to the similar pattern of *H*, and *L* (Figs. 9b, 9d); *Asym* shows a similar pattern, except for cluster 5, with only positive values of *Asym* compared to the other clusters (Fig. 9h).

5. Discussion

5.1 Driving mechanisms of seafloor incision in the Mazzarrà and Rhis-Nekor prodeltas

The presence of widespread gullies in the two study areas is consistent with the prodelta environment and the flood potential of the Mazzarrà and Rhis-Nekor rivers. The network of gullies could result from the interaction between sedimentary gravity flows and the seafloor, as documented elsewhere (e.g., Field et al., 1999; Mitchell et al., 2005; Piper and Normark, 2009; Chiocci and Casalbore, 2001; Casalbore et al., 2011; Shumsker et al., 2017). In particular, the hypothesis of hyperpycnal flows caused by flash-floods is supported by the regional hydrographical setting in the two study areas, since the Rhis, Nekor and Mazzarrà Rivers all have a relatively steep drainage basin (from 1.5° to 4.9° on average), with seasonal hydrological regimes prone to frequent catastrophic flash-floods (Llasat et al., 2010; Casalbore et al., 2017). This is also confirmed

by applying the empirical model of Mulder and Syvitski (1995; Appendix SM1, Eq. 3 and 4), which classifies the Nekor River as a "moderately dirty river", able to generate hyperpycnal flows with a return period of fewer than 100 years (Table 1 and Appendix SM1).

The same empirical approach cannot be applied to the Rhis and Mazzarrà rivers because some input data were not available. However, the Rhis River can be considered a "moderately dirty river" based on its proximity to the Nekor River and similar drainage basin and steep course. Accordingly, the comparison of time-lapse aerial photos at the mouth of these rivers shows a rapid morphological change during and after the main flash-flood events, with the alternation of prograding and erosion stages (Figs. 10a, 10b, 10c, 10d). Similar considerations also apply to the even steeper and shorter Mazzarrà River (Table 1), which is representative of a river type locally known as "fiumara".This kind of river typically drains the Apennine flanks that descend abruptly towards the coastal areas and can transport a considerable amount of debris into the sea in a very short time (Milliman and Syvitski, 1992; Sabato and Tropeano 2004; Gamberi et al., 2014; Chiocci and Casalbore, 2017), resulting in rapid progradation of the coastal delta (Figs. 10e, 10f). In this context, the formation of proto-gully just off a "fiumara-like" river occurred during the 2009 flash-flood event in the nearby western Messina Strait (Casalbore et al., 2011). In different settings, hyperpycnal flows can be generated also by settling of sediment from more dilute river plume, without reaching the critical concentration of 35 – 45 kg/m^3 needed to produce plunging river plume from the source mouth (Lintern et al., 2016; Hizzett et al., 2018; Hage et al., 2019). This implies that hyperpycnal flows can occur at higher frequency because generated by more than one mechanism. Although not documented, a similar process would account for the great number of submarine gullies observed in both study areas.

Despite the similar origin of the gullies in the Rhis-Nekor and Mazzarrà prodeltas, there are some differences in their spatial distribution that likely reflect local geographic and geomorphic aspects. One main difference is in the distance from the coast at which the gullies start to form, 3 km offshore the Rhis-Nekor rivers and only 1 km in front of the Mazzarrà River. Interestingly, this difference in distance turns into a bathymetric compensation since, in both areas, the ensuing gully incision occurs at 30-40 m wd. This coincidence, can be interpreted as an indication (all other factors being similar) of a threshold at which the river plumes generated by the Mazzarrà and Rhis-Nekor rivers become unstable and plunge, forming a sedimentary gravity flow able to shape the seafloor, as modeled by Akiyama and Stefan (1984). This threshold is in the

order of tens of meters in the case of huge sediment discharge (Lamb et al., 2009), which can be expected in both study areas during severe flash-floods according to historical data (Table 1). The ratio between the plunge depth and the average shelf gradients directly controls the distance of the plunging point from the shoreline (which also depends on river discharge, sediment concentration, and lateral spreading of the plume; Johnson et al., 1987; Kassem et al., 2003; Lamb et al., 2009 and 2010). Taking all of the above factors into consideration, the shorter distance to the plunging point in the Mazzarrà prodelta may reflect the steeper shelf gradients (average value 1.5°) compared to the Rhis-Nekor prodelta (average value 0.8°). Alternatively, this depth range can be related to the storm wave base, leading to the obliteration of these morphologies at shallower water depths. A similar smooth morphology has been observed in the upper part of the Fraser prodelta, which aggrades more quickly than the lower part, where similar bedforms are preserved (Hill and Lintern, 2021). However, in this case, the key factor in regulating the different sediment delivery to the submarine slope is tidal amplitude rather than storm waves.

In the Rhis-Nekor prodelta, the gullies occur over a larger area and are generally well spaced, albeit a converging geometry is observed in shallow water near the Rhis River mouth. The converging trend is likely driven by the slightly concave-seaward shape of the bathymetric contour in this area (Figs. 3b, 3d). The wider dispersal of the gullies on the shelf may reflect more frequent migrations of the mouths of the Rhis-Nekor rivers within a wider coastal plain (~ 12 km) where lateral shift and avulsion processes are less contrasted (Fig. 1b).

Conversely, in the Mazzarrà prodelta, the gullies cover a smaller area with an overall radial configuration of the river mouth, likely more steady within its narrower (2 km wide) coastal plain, notwithstanding the very recent anthropic modifications (Figs. 3a, 3c). This distribution can also be linked to the convex-seaward shape of the prodelta, further favoring radial dispersion of the sedimentary gravity flows. It is noteworthy that in the Mazzarrà prodelta, we observe the presence of U-shaped gullies in the proximal part, evolving seaward into narrower and mostly V-shaped gullies that generally tend to fade out rapidly. This could reflect a change in the erosive-depositional behavior of the sedimentary gravity flows, with the U-shaped channels mostly representing a bypass area for the hyperpycnal flows. Once the hyperpycnal flows bypass the proximal shelf, they progressively lose energy, as evidenced by the marked decrease in the incision depth of the mid-shelf gullies and the very small number of gullies that reach the outer shelf (Fig. S4 in

supplementary material). Larger and deeper-cutting gullies develop only along the steeper shelf edge (Figs. 3c and 4a), where the abrupt increase in slope may accelerate residual flows and renew their erosional potential (Fig. S4, Table S1), also favored by the retrogressive erosion that commonly affects shelf breaks (Casalbore et al., 2020). The shelf-break effect resulting in the transient sedimentary gravity flows acceleration appears more evident in the Mazzarrà prodelta, where the gradients are steeper (Figs. 4a, 4b). This acceleration can then form crescent-shaped bedforms in an upper-flow regime within the larger gullies cutting downslope (Slope undulations in Fig. 3c; Kostic et al., 2019).

5.2 Driving mechanism of sediment undulations in the Mazzarrà and Rhis-Nekor prodeltas

In the two study areas, the crests of the undulations run parallel to the bathymetric contour, pointing to the main role of gravity-driven processes in their formation, thereby allowing us to abandon a hypothetical role of along-shelf bottom currents, which would have caused a different elongation trend (Trincardi and Normark, 1988; Diaz and Ercilla 1993; Ercilla et al. 1995; Berndt et al., 2006; Puig et al., 2007; Ercilla et al., 2019).

In-situ sediment deformation (creep) is consistent with the orientation of sediment undulations relative to contour gradients, representing a plausible alternative mechanism since both areas are high sedimentation environments located in seismically active areas (Calvert et al., 1997; Cultrera et al., 2016; Lafosse et al., 2017). The presence of fluid-charged sediment observed down to the base of the HST in the Mazzarrà and Rhis-Nekor prodeltas (Figs. 5a, 5b) could have favored the development of weak layers that enhance the creep of overlying sediments (Hampton et al., 1996; Correggiari et al., 2001; Sultan et al., 2008).

However, apart from these general observations, there is no specific evidence in our data that allows us to infer ongoing creep processes, and the undulated pattern alone is not unequivocal. On the contrary, some specific pieces of evidence favor depositional growth of sediment undulations. For instance, the frequent landward directed asymmetry of the undulations (Figs. 6d and 7d) suggests overall upslope migration, which, in turn, is consistent with sediment gravity flows (Lee et al., 2002; Levchenko and Roslyakov, 2010; Migeon et al., 2001; Bárcenas et al., 2017; Lintern et al., 2016). In this view, the widespread occurrence of gullies in

the two study areas suggests that sedimentary gravity flows capable of reworking the seafloor have been generated directly by the Mazzarrà and Rhis-Nekor rivers (plunging process) or indirectly by the settling from dilute surface plume and/or delta instability processes (Fig. 10).

From a stratigraphic point of view, the seismic profiles in the Gulf of Patti provide evidence for the presence of distinct generations of sediment undulations separated by plane-parallel reflectors (Fig. 5a). This pattern is consistent with a recurrent high-energy driving mechanism alternating with low energy sediment deposition intervals rather than with a creep mechanism, which would require undulations to be continuous above a basal sliding surface (Sultan et al., 2008). To further weigh any interpretation of the most likely genetic mechanism, we focused on the spatial distribution and cluster analysis of the main morphometric parameters that characterize the geometry of sediment undulations, both the Types A and B (Figs. 6, 7, 8 and 9).

The spatial distribution of the heights (*H*) and aspect ratios (*H/L*) of sediment undulations in the Mazzarrà prodelta shows maximum values that correlate with the present-day (eastern) and abandoned branch (western) location of the Mazzarrà River mouth (Figs. 6a, 6c). This positive correlation indicates a relationship between processes at the river mouth and enhanced growth of sediment undulations, further evidence for the sedimentary gravity flows as the driving genetic mechanism of sediment undulation. A similar correlation has been documented for the Guadalfeo prodelta in southern Iberia, which shares similar aspect ratios with the Verde-Seco and the Mazzarrà prodeltas, and where hyperpycnal flows are considered to be the most plausible mechanism (Fig. 11a) (Fernandez-Salas et al., 2007; Lobo et al. 2015). Comparison with Squamish, Fraser and Noeick prodeltas shows the occurrence of similar gullies and undulations with comparable aspect ratio (Fig. 11 and Table 2). In such cases, undulations have been interpreted as the result of sediment gravity flows associated with plunging flows from the river mouth and/or sediment settling processes from hypopycnal flows (Bornhold and Prior, 1990; Hill, 2012; Hughes Clarke et al., 2012; Hizzet et al., 2018; Hage et al., 2019; Hill et al., 2021).

The above considerations, combined with the importance of the aspect ratio as a genetic indicator (Urgeles et al., 2011), support the hypothesis that hyperpycnal flows are responsible for the formation of sediment undulations in the Mazzarà prodelta. In this view, we observe that the peak values within the greater *H* and *H/L* concentrate immediately in front of Channel A (Ch A in Figs. 6a, 6c), are actually the submarine continuation of the river mouth. Additional geomorphic control resulting from statistical and cluster analysis

is the shelf gradient, because of the shape and overall regular morphology of the prodelta deposits, the shelf gradient mimics a correlation with the distance from the river mouth and, more indirectly, with the thickness of the HST (Figs. 4c and 9a, 9c, 9e).

Concerning a tripartition of the prodelta area into a proximal, middle, and distal sector, the *H* and *H/L* show peak values falling in the middle prodelta (cluster 2 in Figs. 8a and 9a, 9b, 9f). This specific distribution has been documented in other examples of sediment undulations, suggesting a relationship between the dimensional scale of these bedforms and the reciprocal contribution of suspended and bedload transport (Carle and Hill, 2009). The implication is that sedimentary flows may need to travel for some distance over a steepening shelf before fully developing the erosive-depositional potential capable of generating relatively large bedforms (section 5.1 and Figs. 8a and 9b, 9c, 9d, 9f, 9g). Beyond this point, the flows progressively lose energy if they enter an area where gradients decrease downslope (Figs. 4a, 6f, and 9g). Accordingly, in the distal prodelta area, we observe smaller scale sediment undulations (Figs. 6a, 6c and cluster 3 in figs. 8a and 9b, 9d, 9f) associated with less incised, shallower gullies (Fig. S4). A similar down-slope decrease of *H* is not uncommon and has been observed in areas where turbidity currents generate the sediment waves (e.g., Wynn and Stow, 2002; Boe et al., 2004; Urgeles et al., 2007).

In the Al-Hoceima case study, the spatial distribution of the morphometric parameters is less linear with the increasing distance from the rivers mouths, likely reflecting staircase shelf morphology, where the gentle slope of the middle shelf is interrupted by the scarp associated with the submarine terrace (Fig. 4b; blue line in Fig. 7). Cluster analysis (Figs. 8b and 9) indicates that the higher *H* and *L* values are reached in the proximal sector of the prodelta facing the mouths of the Rhis-Nekor rivers (cluster 5 in Figs. 8b and 9), with patches in the proximal-mid and mid-distal transitional areas (just downslope of the morphological scarp; cluster 7 in Figs. 8b and 9). Conversely, sediment undulations with lower *H* and *L* are concentrated upslope of the morphological scarp in the proximal prodelta sector (cluster 4) and outside the Rhis-Nekor prodelta (cluster 6 and 8).

The higher *H* and *L* values in the proximal sector and the proximal-mid transitional area are comparable with the values observed in the same proximal-mid area of the Mazzarrà prodelta (clusters 1, 2, 3 4, 5, 6 in figs. 8b and 9), albeit with clearer mixing of clusters 4 and 5, supporting the role of sedimentary gravity flow in the formation of undulations.

Considering the large number of small and convergent gullies present (Fig. 3b and Table S2), a genetic relationship with sedimentary gravity flows can also be hypothesized in this case. Instead, the concentration of peak values of *H*, *L*, and *H/L* of sediment undulations in the mid-distal Rhis-Nekor prodelta (cluster 7 in Figs. 8b and 9) contrasts with observations in the mid-distal Mazzarrà prodelta and likely reflects a "gradient effect" induced by the morphological scarp. In particular, the abrupt shelf break would trigger hydraulic jumps in sedimentary gravity flows, leading to increased flow thickness and enhanced deposition and growth of sediment undulations.

However, this mechanism is less consistent with the significant increase in the lateral extent (up to few kilometers) of the corresponding sediment undulations (Fig. 7e). Taking all of the above factors into consideration, one way to reconcile the observed morphological pattern with sedimentary gravity flows as a genetic mechanism of sediment undulations is to assume that, in the Rhis-Nekor prodelta, unconfined turbidity currents flowed over most of the distal and low gradient prodelta area.

An alternative mechanism to explain the overwhelming lateral extent of sediment undulations could be the breaking of internal waves (Puig et al., 2007; Van Haren and Puig, 2017), as observed in other micro-tidal environments (i.e., Ribó et al., 2016 and reference therein; Urgeles et al., 2011). For example, the *H/L* of the undulations in the Rhis-Nekor prodelta are similar to that of the Llobregat and Adriatic undulations (Fig. 11b and Table 2), which are referred to as hyperpycnal flows and internal waves (Urgeles et a., 2007; Van Haren and Piug, 2017) or soft-sediment deformation and bottom currents (Cattaneo et al., 2004; Sultan et al., 2008), respectively. Internal wave dynamics, although difficult to address with our data, are documented for the Moroccan shelf (Ercilla et al., 2016; Van Haren and Puig, 2017), and would be consistent with the increase in the lateral extent of the sediment undulations on the outer shelf. During a cruise perfomed in the Al-Hoceima Bay in November 2021, internal waves were recorded at approximately 120 m wd (unpublished data). In addition, recent studies have shown that the depth range of the thermocline offshore Marocco is comprised between 50 and 200 m (Nibani et al., 2021), where we would expect the peak of internal wave activity. Moreover, it has been shown elsewhere that river plumes into the sea can generate large-amplitude internal waves (Nash and Moum, 2005). In more detail, the lower *H/L* ratios correspond to the similar trend of *L* and *H* values of undulations in the Rhis-Nekor, differently from what was observed in the Mazzarrà prodelta (Figs. 9b, 9d, 9f). This likely reflects the more regular shape of the undulations in the Rhis-Nekor

prodelta, especially on the middle and outer shelf (Figs. 3b, 3d), which, in turn, may be controlled by unconfined sedimentary flows and/or internal waves. In the Mazzarrà prodelta, the higher *H/L* values are instead due to a uniform distribution of L and non-uniform of H values within the three clusters (Figs. 6b, 9b, 9d, 9f). This is likely due to the superimposition of smaller bedforms over larger ones (Figs. 3c and S3), and the difficulty in resolving them, by this affecting the correct measurement of wavelengths. In turn, the superposition of different scale undulations may reflect the the greater variability in size and energy of hyperpycnal flows formed at the mouth of the Mazzarrà River.

5.3 Coexistence of gullies and sediment undulations

The coexistence of gullies and sediment undulations observed in the Rhis-Nekor and Mazzarrà prodeltas is not commonly observed in other Mediterranean prodeltas (Urgeles et al., 2011; Barcenas et al., 2015). Based on known constraints, gullies have been associated with the erosion exerted by sedimentary gravity flows on the seafloor. The undulations can be similarly interpreted as the results of erosive-depositional processes associated with sedimentary gravity flow (sections 5.1 and 5.2), or even due to other mechanisms, such as creep and breaking of internal waves (especially in the case of the large bedforms identified in the distal part of the Rhis-Nekor prodelta). In the latter cases, the coexistence of gullies and undulations results from different well-understood processes. The genetic relationship between these bedforms are more difficult to explain if they are generated by the same process, namely sedimentary gravity flows. In this view, two main hypotheses can be proposed. First, gullies and sediment undulations are different effects of flow behavior during flood events and/ or ponding process from dilute plume, such as centrifugal instabilities that develop at the interface of unconfined gravity currents as they flow through a change in slope gradients (Fedele and Garcia; 2009). These would cause the destabilization and fingering of sedimentary gravity flows (Parson et al., 2007) with the formation of zones with increased erosion (gullies) and deposition (sediment undulations). Second, gullies are ephemeral features resulting from a single or a few events when the riverine flow is more concentrated and able to erode the seafloor, whereas the sediment undulations are rather the result of the stacking of multiple and unconfined gravity flows in which the supply of sediment plays a key role. The latter inference could also explain why prodeltas with undulations and gullies exist off the Mazzarrà and Rhis-Nekor outlets, whereas shallow gullies with few undulations are observed off smaller river courses

(Elicona River in the Gulf of Patti and ephemeral small river networks in Al-Hoceima Bay in Figs. 1a, 1b, and 3c, 3d, respectively).

Conclusion

The Mazzarrà and Rhis-Nekor prodeltas are characterized by the coexistence of gullies and undulations from the inner shelf to the shelf break, a characteristic that is relatively rare in other Mediterranean prodeltaic systems.

In both case studies, the gullies are considered ephemeral features and interpreted as the result of erosion of the seafloor due to the passage of flash-flood hyperpycnal flows, favored by the steep drainage basin and torrential regimes of the Mazzarrà, Rhis and Nekor Rivers (Fig. 12). Gullies generally become wider and deeper due to the marked increase in slope gradients. This process is clearly evidenced at-or close to the shelf break, often producing retrogressive erosion. The plan-view pattern of the gullies is primarily controlled by shelf morphology and by the main characteristics of the alluvial plain.

The interpretation of seafloor undulations is still the subject of debate, but our analysis supports a main role for erosive-depositional processes due to sediment gravity flows in both the study areas, even though the breaking of internal waves in the mid-distal part of the Rhis-Nekor prodelta cannot be excluded. This additional process would be consistent with the distribution of the wave heights, aspect ratio, and lateral extent of the undulations on the outer shelf. Also in this case, shelf morphology and in particular, slope gradients remain key factors in controlling the development of seafloor undulations. However, the question that remains is how sedimentary dynamics control the coexistence of gullies and undulations if both features are associated with the activity of sedimentary gravity flows. In this study, two main mechanisms have been advocated: (i) centrifugal instabilities within the flows or (ii) seafloor undulations can be considered as the result of the stacking of multiple gravity flows triggered by shallow slide scars and/or flood events, whereas gullies are linked to the one (or few) event(s) able to erode the seafloor, thus representing ephemeral features.

More generally, our results show that it is possible to compare undulations in different areas based on a small number of morphometric characteristics. In particular, the aspect ratio (i.e., the ratio between wave height and wavelength) is useful to compare seafloor undulations (Fig. 11), but alone, this parameter is not

sufficient to clearly define the processes that determine their creation. It is also necessary to consider the marked variation in the controlling factors in different prodeltas, such as slope gradient, shelf morphology and river supply dynamics, which control the dispersion, recurrence and energy of sedimentary gravity flows and hence the development of the associated bedforms. Moreover, high-resolution seismo-stratigraphic and sedimentogical analyses could better explain the origin of these features, as for instance demonstrated by the seismic profiles available for the Mazzarrà case study.

Acknowledgments

This research was funded by the Italian Project MaGIC (Marine Geohazards along the Italian Coasts), and by the French program *Actions Marges*, the EUROFLEETS program (FP//2007-2013; n°228344), project FICTS-2011-03-01, and ALBAMAR JCJC ANR-17-CE03-0004. The processed seismic data were interpreted using Kingdom IHS Suite© software. Our special thanks go to the crews of R/V Urania, Minerva Uno (CNR) and R/V "Téthys II" (CNRS-INSU) and to the participants in the marine surveys. (https://doi.org/10.17600/12450090, and https://campagnes.flotteoceanographique.fr/campagnes/12000010). We thank the Editor David Kennedy and the reviewers Tiago M. Alves and John Hughes Clarke for their insightful comments and suggestions.

References

Abdalla, F., El Shamy, I., Bamousa, A. O., Mansour, A., Mohamed, A., Tahoon, M., 2014. Flash floods and groundwater recharge potentials in arid land alluvial basins, southern Red Sea coast, Egypt. Int. J. Geosci. 5(09), 971. https://doi.org/10.4236/ijg.2014.59083.

Akiyama, J., Stefan, H. G., 1984. Plunging flow into a reservoir: Theory. J. Hydraul. Eng. 110(4), 484-499. https://doi.org/10.1061/(ASCE)0733-9429(1984)110:4(484).

Amil M., 1992. Bassin versant du Nekor recherché des zones sources d'envasement de la retenue du barrage M.B.A. El-Khettabi (Maroc), These.

Bárcenas, P., Fernández-Salas, L. M., Macías, J., Lobo, F. J., Díaz del Río, V., 2009. Estudio morfométrico comparativo entre las ondulaciones de los prodeltas de los ríos de Andalucía Oriental. Rev. Soc. Geol. Esp. 22(1-2), 43-56.

Bárcenas, P., Lobo, F. J., Fernández-Salas, L. M., Ortega-Sánchez, M., Mendes, I., Macías, J., 2017. Prodeltaic undulations and hyperpycnal flows (i): morphological observations. In Atlas of Bedforms in the Western Mediterranean, Springer, Cham. pp. 107-112. https://doi.org/10.1007/978-3-319-33940-5_18.

Barcos, L., Jabaloy, A., Azdimousa, A., Asebriy, L., Gómez-Ortiz, D., Rodríguez-Peces, M. J., Pérez-Peña, J. V., 2014. Study of relief changes related to active doming in the eastern Moroccan Rif (Morocco) using geomorphological indices. J. Afr. Earth Sci. 100, 493-509. https://doi.org/10.1016/j.jafrearsci.2014.07.014.

Bassetti, M. A., Jouet, G., Dufois, F., Berné, S., Rabineau, M., Taviani, M., 2006. Sand bodies at the shelf edge in the Gulf of Lions (Western Mediterranean): Deglacial history and modern processes. Mar. Geol. 234(1-4), 93-109. https://doi.org/10.1016/j.margeo.2006.09.010.

Bellotti, P., Chiocci, F. L., Milli, S., Tortora, P., Valeri, P., 1994. Sequence stratigraphy and depositional setting of the Tiber Delta; integration of high-resolution seismics, well logs, and archeological data. J. Sediment. Res. 64(3b), 416-432. https://doi.org/10.1306/D4267FDC-2B[illegible]-11D7-8648000102C1865D.

Berndt, C., Cattaneo, A., Szuman, M., Trincardi, F., Masson, D., 2006. Sedimentary structures offshore Ortona, Adriatic Sea—Deformation or sediment waves?. Mar. Geol. 234(1-4), 261-270. https://doi.org/10.1016/j.margeo.2006.09.016.

Bøe, R., Bugge, T., Rise, L., Eidnes, G., Eide, A., Mauring, E., 2004. Erosional channel incision and the origin of large sediment waves in Trondheimsfjorden, central Norway. Geo-Mar Lett. 24(4), 225-240. https://doi.org/10.1007/s00367-004-0180-3.

Bornhold, B. D., Prior, D. B., 1990. Morphology and sedimentary processes on the subaqueous Noeick River delta, British Columbia, Canada. In Coarse-grained deltas (Vol. 10, pp. 169-181). Oxford, UK: Blackwell Scientific Publications. https://doi.org/10.1002/9781444303858.ch9.

Calvert, A., Gomez, F., Seber, D., Barazangi, M., Jabour, N., Ibenbrahim, A., Demnati, A., 1997. An integrated geophysical investigation of recent seismicity in the Al-Hoceima region of North Morocco. Bull. Seismol. Soc. Am. 87(3), 637-651.

Carle, L., Hill, P. R., 2009. Subaqueous dunes of the upper slope of the Fraser River Delta (British Columbia, Canada). J. Coastal Res. 25(2 (252)), 448-458. https://doi.org/10.2112/06-0796.1.

Casalbore, D., Chiocci, F. L., Mugnozza, G. S., Tommasi, P., Sposato, A., 2011. Flash-flood hyperpycnal flows generating shallow-water landslides at Fiumara mouths in Western Messina Strait (Italy). Mar. Geophys. Res. 32(1-2), 257. https://doi.org/10.1007/s11001-011-9128-y.

Casalbore, D., Ridente, D., Bosman, A., Chiocci, F. L., 2017. Depositional and erosional bedforms in Late Pleistocene-Holocene pro-delta deposits of the Gulf of Patti (southern Tyrrhenian margin, Italy). Mar. Geol. 385, 216-227. https://doi.org/10.1016/j.margeo.2017.01.007

Casalbore, D., Clementucci, R., Bosman, A., Chiocci, F. L., Martorelli, E., Ridente, D., 2020. Widespread mass-wasting processes off NE Sicily (Italy): insights from morpho-bathymetric analysis. Geol. Soc. London, Spec. Publ. 500(1), 393-403. https://doi.org/10.1144/SP500-2019-195

Cattaneo, A., Correggiari, A., Marsset, T., Thomas, Y., Marsset, B., Trincardi, F., 2004. Seafloor undulation pattern on the Adriatic shelf and comparison to deep-water sediment waves. Mar. Geol. 213(1-4), 121-148. https://doi.org/10.1016/j.margeo.2004.10.004.

Chafouq, D., El Mandour, A., Elgettafi, M., Himi, M., Chouikri, I., Casas, A., 2018. Hydrochemical and isotopic characterization of groundwater in the Ghis-Nekor plain (northern Morocco). J. Afr. Earth Sci. 139, 1-13. https://doi.org/10.1016/j.jafrearsci.2017.11.007.

Chalouan, A., Michard, A., El Kadiri, K., Negro, F., De Lamotte, D. F., Soto, J. I., Saddiqi, O., 2008. The Rif Belt. In Continental evolution: the geology of Morocco (pp. 203-302). Springer, Berlin, Heidelberg. https://doi.org/10.1007/978-3-540-77076-3_5.

Chiarabba, C., Jovane, L., DiStefano, R., 2005. A new view of Italian seismicity using 20 years of instrumental recordings. Tectonophysics. 395(3-4), 251-268. https://doi.org/10.1016/j.tecto.2004.09.013.

Chiocci, F. L., Normark, W. R., 1992. Effect of sea-level variation on upper-slope depositional processes offshore of Tiber delta, Tyrrhenian Sea, Italy. Mar. Geol. 104(1-4), 109-122. https://doi.org/10.1016/0025-3227(92)90087-X.

Chiocci, F.L., Esu, F., Tommasi, P., Chiappa, V., 1996. Stability of the submarine slope of the Tiber River delta. In: Senneset K (ed) Landslides. Balkema, The Netherlands., pp 521–526.

Chiocci, F. L., Casalbore, D., 2011. Submarine gullies on Italian upper slopes and their relationship with volcanic activity revisited 20 years after Bill Normark's pioneering work. Geosphere. 7(6), 1284-1293. https://doi.org/10.1130/GES00633.1.

Chiocci, F. L., Casalbore, D., 2017. Unexpected fast rate of morphological evolution of geologically-active continental margins during Quaternary: Examples from selected areas in the Italian seas. Mar. Petrol. Geol. 82, 154-162. https://doi.org/10.1016/j.marpetgeo.2017.01.025.

Correggiari, A., Trincardi, F., Langone, L., Roveri, M., 2001. Styles of failure in late Holocene highstand prodelta wedges on the Adriatic shelf. J. Sediment. Res. 71(2), 218-236. https://doi.org/10.1306/042800710218.

Cuffaro, M., Riguzzi, F., Scrocca, D., Doglioni, C., 2011. Coexisting tectonic settings: the example of the southern Tyrrhenian Sea. Int. J. Earth Sci. 100(8), 1915-1924. https://doi.org/10.1007/s00531-010-0625-z.

Cultrera, F., Barreca, G., Burrato, P., Ferranti, L., Monaco, C., Passaro, S., Pepe, F., Scarfì, L., 2017. Active faulting and continental slope instability in the Gulf of Patti (Tyrrhenian side of NE Sicily, Italy): a field, marine and seismological joint analysis. Nat. Hazards 86(2), 253-272. https://doi.org/10.1007/s11069-016-2547-y.

d'Acremont, E., Gutscher, M. A., Rabaute, A., de Lépinay, B. M., Lafosse, M., Poort, J., Ammar, A., Tahayt, A., Le Roy, P., Smit, J., Do Couto, D., Cancouët, R., Prunier, C., Ercilla, G., Gorini, C., 2014. High-resolution imagery of active faulting offshore Al Hoceima, Northern Morocco. Tectonophysics. 632, 160-166. https://doi.org/10.1016/j.tecto.2014.06.008.

De Guidi, G., Lanzafame, G., Palano, M., Puglisi, G., Scaltrito, A., Scarfì, L., 2013. Multidisciplinary study of the Tindari Fault (Sicily, Italy) separating ongoing contractional and extensional compartments along the active Africa–Eurasia convergent boundary. Tectonophysics 588, 1-17. https://doi.org/10.1016/j.tecto.2012.11.021.

Díaz, J. I., Ercilla, G., 1993. Holocene depositional history of the Fluviá—Muga prodelta, northwestern Mediterranean Sea. Mar. Geol., 111(1-2), 83-92. https://doi.org/10.1016/0025-3227(93)90189-3.

Duchesne, M. J., Long, B. F., Urgeles, R., Locat, J., 2002. New evidence of slope instability in the Outardes Bay delta area, Quebec, Canada. Geo-Mar. Lett. 22(4), 233-242. https://doi.org/10.1007/s00367-003-0121-6.

El Alami, S. O., Tadili, B. A., Cherkaoui, T. E., Medina, F., Ramdani, M., Brahim, L. A., Harnafi, M., 1998. The Al Hoceima earthquake of May 26, 1994 and its aftershocks: a seismotectonic study. Ann. Geofis. 41(4). https://doi.org/10.4401/ag-3801.

Ercilla, G., Díaz, J. I., Alonso, B., Farran, M., 1995. Late Pleistocene-Holocene sedimentary evolution of the northern Catalonia continental shelf (northwestern Mediterranean Sea). Cont. Shelf Res. 15(11-12), 1435-1451. https://doi.org/10.1016/0278-4343(94)00089-6.

Ercilla, G., Juan, C., Hernandez-Molina, F. J., Bruno, M., Estrada, F., Alonso, B., Casas, D., Farran, M., Llave, E., García, M., Vázquez, J.T., D'Acremont, E., Gorini, C., Palomino, D., Valencia, J., El Moumni, B., Ammar, A., 2016. Significance of bottom currents in deep-sea morphodynamics: an example from the Alboran Sea. Mar. Geol. 378, 157-170. https://doi.org/10.1016/j.margeo.2015.09.007.

Ercilla, G., Juan, C., Periáñez, R., Alonso, B., Abril, J. M., Estrada, F., Casas D., Vázquez J.T., d'Acremont E., Gorini C., El Moumni B., Do Couto D., Valencia, J., 2019. Influence of alongslope processes on modern turbidite systems and canyons in the Alboran Sea (southwestern Mediterranean). Deep-Sea Res. I Oceanogr. Res. Pap. 144, 1-16. https://doi.org/10.1016/j.dsr.2018.12.002

Faccenna, C., Becker, T. W., Lucente, F. P., Jolivet, L., Rossetti, F., 2001. History of subduction and back arc extension in the Central Mediterranean. Geophys. J. Int. 145(3), 809-820. https://doi.org/10.1046/j.0956-540x.2001.01435.x.

Fedele, J. J., García, M. H., 2009. Laboratory experiments on the formation of subaqueous depositional gullies by turbidity currents. Mar. Geol. 258(1-4), 48-59. https://doi.org/10.1016/j.margeo.2008.11.004.

Fernández-Salas, L. M., Lobo, F. J., Sanz, J. L., Díaz-del-Río, V., García, M. C., Moreno, I., 2007. Morphometric analysis and genetic implications of pro-deltaic sea-floor undulations in the northern Alboran Sea margin, western Mediterranean Basin. Mar. Geol. 243(1-4), 31-56. https://doi.org/10.1016/j.margeo.2007.04.013.

Ferranti, L., Antonioli, F., Anzidei, M., Monaco, C., Stocchi, P., 2010. The timescale and spatial extent of vertical tectonic motions in Italy: insights from relative sea-level changes studies. J. Virtual Explor. 36(Paper 30). https://doi.org/10.3809/jvirtex.2010.00255.

Field, M. E., Gardner, J. V., Prior, D. B., 1999. Geometry and significance of stacked gullies on the northern California slope. Mar. Geol. 154(1-4), 271-286. https://doi.org/10.1016/S0025-3227(98)00118-2.

Flood, R. D, 1981. Distribution, morphology, and origin of sedimentary furrows in cohesive sediments, Southampton Water. Sedimentology. 28(4), 511-529. https://doi.org/10.1111/j.1365-3091.1981.tb01699.x.

Gamberi, F., Rovere, M., Mercorella, A., Leidi, E., Dalla Valle, G., 2014. Geomorphology of the NE Sicily continental shelf controlled by tidal currents, canyon head incision and river-derived sediments. Geomorphology. 217, 106-121. https://doi.org/10.1016/j.geomorph.2014.03.038.

Gascard, J. C., Richez, C., 1985. Water masses and circulation in the western Alboran Sea and in the Straits of Gibraltar. Prog. Oceanogr. 15(3), 157-216. https://doi.org/10.1016/0079-6611(85)90031-X.

Girardclos, S., Hilbe, M., Corella, J. P., Loizeau, J. L., Kremer, K., DelSontro, T., Arantegui A., Moscariello A., Arlaud F., Akhtman Y., Anselmetti, F.S., Lemmin, U., 2012. Searching the Rhone delta channel in Lake

Geneva since François Alphonse FOREL. Archives des Sciences. 65, 103-118. https://doi.org/10.3997/2214-4609.201412970.

Hage, S., Cartigny, M. J., Sumner, E. J., Clare, M. A., Hughes Clarke, J. E., Talling, P. J., Lintern, G., Simmons, S., Jacinto, R.S., Vellinga, A.J., Allin, J.R., Azpiroz-Zabala, M., Gales, J.A., Hizzett, L., Hunt, J.E.,Mozzato, A., Parsons, D.R., Pope, L., Stacey, C.D., Symons, W.O., Vardy, M.E., Watts, C., 2019. Direct monitoring reveals initiation of turbidity currents from extremely dilute river plumes. Geophys. Res. Lett. 46(20), 11310-11320. https://doi.org/10.1029/2019GL084526

Hampton, M. A., Lee, H. J., Locat, J., 1996. Submarine landslides. Rev. Geophys. 34(1), 33-59. https://doi.org/10.1029/95RG03287.

Hill, P. R., Li, M. Z., Sherwood, C. R., 2012. Changes in submarine channel morphology and slope sedimentation patterns from repeat multibeam surveys in the Fraser River delta, western Canada. Int. Assoc. Sedimentol. Spec. Publ. 44, 47-70. https://doi.org/10.1002/9781118311172.ch3.

Hill, P. R., Lintern, D. G., 2021. Sedimentary processes at the mouth of a tidally-influenced delta: New insights from submarine observatory measurements, Fraser Delta, Canada. Sedimentology. 68(6), 2649-2670. https://doi.org/10.1111/sed.12868.

Hizzett, J. L., Hughes Clarke, J. E., Sumner, E. J., Cartigny, M. J. B., Talling, P. J., Clare, M. A., 2018. Which triggers produce the most erosive, frequent, and longest runout turbidity currents on deltas?. Geophys. Res. Lett. 45(2), 855-863. https://doi.org/10.1002/2017GL075751.

Hughes Clarke, J., Brucker, S., Muggah, J., Church, I., Cartwright, D., Kuus, P., Hamilton, T., Pratomo, D., Eisan, B., 2012. The Squamish ProDelta: monitoring active landslides and turbidity currents. In Canadian Hydrographic Conference 2012, Proceedings (p. 15).

Istituto Idrografico della Marina, 1982. Atlante delle correnti superficiali dei mari d'Italia. 1st. Idrogr. 3068. Mar. Publ. Genova.

Johnson, T. R., Farrell, G. J., Ellis, C. R., Stefan, H. G., 1987. Negatively buoyant flow in a diverging channel. I: Flow regimes. J. Hydraul. Eng. 113(6), 716-730.

Juan, C., Ercilla, G., Hernández-Molina, F. J., Estrada, F., Alonso, B., Casas, D., Garcia M., Farran, M., Llave E., Palomino D., Vasquez, J.T., Medialdea T., Gorini C., d'Acremont E., Al Moumni B., Ammar, A., 2016. Seismic evidence of current-controlled sedimentation in the Alboran Sea during the Pliocene and Quaternary: Palaeoceanographic implications. Mar. Geol. 378, 292-311. https://doi.org/10.1016/j.margeo.2016.01.006.

Kassem, A., Imran, J., Khan, J. A., 2003. Three-dimensional modeling of negatively buoyant flow in diverging channels. J. Hydraul. Eng. 129(12), 936-947. https://doi.org/10.1061/(ASCE)0733-9429(2003)129:12(936).

Khouakhi, A., Snoussi, M., Niazi, S., Raji, O., 2013. Vulnerability assessment of Al Hoceima bay (Moroccan Mediterranean coast): a coastal management tool to reduce potential impacts of sea-level rise and storm surges. J. Coastal Res. (65), 968-973. https://doi.org/10.2112/SI65-164.1

Kostic, S., Casalbore, D., Chiocci, F., Lang, J., Winsemann, J., 2019. Role of upper-flow-regime bedforms emplaced by sediment gravity flows in the evolution of deltas. J. Mar. Sci. Eng. 7(1), 5. https://doi.org/10.3390/jmse7010005.

Lafosse, M., d'Acremont, E., Rabaute, A., Mercier de Lépinay, B., Tahayt, A., Ammar, A., Gorini, C., 2017. Evidence of Quaternary transtensional tectonics in the Nekor basin (NE Morocco). Basin Res. 29(4), 470-489. https://doi.org/10.1111/bre.12185.

Lafosse, M., Gorini, C., Le Roy, P., Alonso, B., d'Acremont, E., Ercilla, G, Rabineau, M., Vasquez, J.T., Rabaute A., Ammar, A., 2018. Late Pleistocene-Holocene history of a tectonically active segment of the continental margin (Nekor basin, Western Mediterranean, Morocco). Mar. Petrol. Geol. 97, 370-389. https://doi.org/10.1016/j.marpetgeo.2018.07.022.

Lamb, M. P., Mohrig, D., 2009. Do hyperpycnal-flow deposits record river-flood dynamics?. Geology, 37(12), 1067-1070. https://doi.org/10.1130/G30286A.1.

Lamb, M. P., McElroy, B., Kopriva, B., Shaw, J., Mohrig, D., 2010. Linking river-flood dynamics to hyperpycnal-plume deposits: Experiments, theory, and geological implications. GSA Bulletin, 122(9-10), 1389-1400. https://doi.org/10.1130/B30125.1.

Lee, H. J., Syvitski, J. P., Parker, G., Orange, D., Locat, J., Hutton, E. W., Imran, J., 2002. Distinguishing sediment waves from slope failure deposits: field examples, including the 'Humboldt slide', and modelling results. Mar. Geol. 192(1-3), 79-104. https://doi.org/10.1016/S0025-3227(02)00550-9.

Lentini, F., Catalano, S., Carbone, S., 1996. The external thrust system in southern Italy; a target for petroleum exploration. Petrol. Geosci. *2*(4), 333-342. https://doi.org/10.1144/petgeo.3.3.285.

Lentini, F., Carbone, S., Guarnieri, P., Dilek, Y., Pavlides, S., 2006. Collisional and postcollisional tectonics of the Apenninic-Maghrebian orogen (southern Italy). Geol. S Am. S. 409, 57. https://doi.org/10.1130/2006.2409(04).

Levchenko O.V., Roslyakov A.G., 2010. Cyclic sediment waves on western slope of the Caspian Sea as possible indicators of main transgressive/regressive events. Quat. Int. 225(2):210–220. doi:10.1016/j.quaint.2009.12.001. https://doi.org/10.1016/j.quaint.2009.12.001.

Li, W., Alves, T. M., Wu, S., Rebesco, M., Zhao, F., Mi, L., Ma, B., 2016. A giant, submarine creep zone as a precursor of large-scale slope instability offshore the Dongsha Islands (South China Sea). Earth Planet. Sci. Lett. 451, 272-284. https://doi.org/10.1016/j.epsl.2016.07.007.

Li, J., Li, W., Alves, T. M., Rebesco, M., Zhan, W., Sun, J., Mitchell C., Wu, S., 2019. Different origins of seafloor undulations in a submarine canyon system, northern South China Sea, based on their seismic character and relative location. Mar. Geol. 413, 99-111. https://doi.org/10.1016/j.margeo.2019.04.007.

Lintern, D. G., Hill, P. R., Stacey, C., 2016. Powerful unconfined turbidity current captured by cabled observatory on the Fraser River delta slope, British Columbia, Canada. Sedimentology. 63(5), 1041-1064. https://doi.org/10.1111/sed.12262.

Llasat, M. C., Llasat-Botija, M., Prat, M. A., Porcú, F., Price, C., Mugnai, A., Lagouvardos, K., Kotroni, V., Katsanos, D., Michaelides, S., Yair, Y., Savvidou, K., Nicolaides, K., 2010. High-impact floods and flash floods in Mediterranean countries: the FLASH preliminary database. Adv. Geosci. 23, 47-55. https://doi.org/10.5194/adgeo-23-47-2010.

Lobo, F. J., Ridente, D., 2014. Stratigraphic architecture and spatio-temporal variability of high-frequency (Milankovitch) depositional cycles on modern continental margins: an overview. Mar. Geol. 352, 215-247. https://doi.org/10.1016/j.margeo.2013.10.009.

Lobo, F. J., Goff, J. A., Mendes, I., Bárcenas, P., Fernández-Salas, L. M., Martín-Rosales, W., Macías, J., Del Río, V. D., 2015. Spatial variability of prodeltaic undulations on the Guadalfeo River prodelta: support to the genetic interpretation as hyperpycnal flow deposits. Mar. Geophys. Res. 36(4), 309-333. https://doi.org/10.1007/s11001-014-9233-9.

Lykousis, V., Roussakis, G., Sakellariou, D., 2009. Slope failures and stability analysis of shallow water prodeltas in the active margins of Western Greece, northeastern Mediterranean Sea. International J. Earth Sci. 98(4), 807-822. https://doi.org/10.1007/s00531-008-0329-9.

Maillet, G. M., Vella, C., Berné, S., Friend, P. L., Amos, C. L., Fleury, T. J., Normand, A., 2006. Morphological changes and sedimentary processes induced by the December 2003 flood event at the present mouth of the Grand Rhône River (southern France). Mar. Geol. 234(1-4), 159-177. https://doi.org/10.1016/j.margeo.2006.09.025.

Migeon, S., Savoye, B., Zanella, E., Mulder, T., Faugères, J. C., Weber, O., 2001. Detailed seismic-reflection and sedimentary study of turbidite sediment waves on the Var Sedimentary Ridge (SE France): significance for sediment transport and deposition and for the mechanisms of sediment-wave construction. Mar. Petrol. Geol. 18(2), 179-208. https://doi.org/10.1016/S0264-8172(00)00060-X.

Milliman, J. D., Syvitski, J. P., 1992. Geomorphic/tectonic control of sediment discharge to the ocean: the importance of small mountainous rivers. J. Geol. 100(5), 525-544. https://doi.org/10.1086/629606.

Mitchell, N. C., 2005. Channelled erosion through a marine dump site of dredge spoils at the mouth of the Puyallup River, Washington State, USA. Mar. Geol. 220(1-4), 131-151. https://doi.org/10.1016/j.margeo.2005.06.032

Morel, J. L., Meghraoui, M., 1996. Goringe-Alboran-Tell tectonic zone: A transpression system along the Africa-Eurasia plate boundary. Geology. 24(8), 755-758. https://doi.org/10.1130/0091-7613(1996)024<0755:GATTZA>2.3.CO;2.

Mulder, T., Syvitski, J. P., 1995. Turbidity currents generated at river mouths during exceptional discharges to the world oceans. J. Geol. 103(3), 285-299. https://doi.org/10.1086/629747.

Nash, J., Moum, J., 2005. River plumes as a source of large-amplitude internal waves in the coastal ocean. Nature. 437**,** 400–403. https://doi.org/10.1038/nature03936.

Nibani, H., Hilmi, K., Damghi, A., Beguery, L., Fommervault, O., Amhaoauch, Z., 2021. Al-Hoceima launches its first functional marine observatory in North Africa. In 9th EuroGOOS International conference. hal-03331067v2.

Parsons, J. D., Friedrichs, C. T., Traykovski, P. A., Mohrig, D., Imran, J., Syvitski, J. P., Parker G., Puig P., Buttles J., Garcia M. H., 2007. The mechanics of marine sediment gravity flows. Continental margin sedimentation: from sediment transport to sequence stratigraphy. IAP Spec. Pub. *37*, 275-334. https://doi.org/10.1002/9781444304398.ch6.

Piper, D. J., Normark, W. R., 2009. Processes that initiate turbidity currents and their influence on turbidites: a marine geology perspective. J. Sediment. Res. 79(6), 347-362. https://doi.org/10.2110/jsr.2009.046.

Poujol, A., Ritz, J. F., Tahayt, A., Vernant, P., Condomines, M., Blard, P. H., Billant, J., Vacher, L., Tidari, B., Hni, L., Idrissi, A. K., 2014. Active tectonics of the Northern Rif (Morocco) from geomorphic and geochronological data. J. Geodyn. 77, 70-88. https://doi.org/10.1016/j.jog.2014.01.004.

Puig, P., Ogston, A. S., Guillén, J., Fain, A. M. V., Palanques, A., 2007. Sediment transport processes from the topset to the foreset of a crenulated clinoform (Adriatic Sea). Cont. Shelf Res. 27(3-4), 452-474. https://doi.org/10.1016/j.csr.2006.11.005.

Ribó, M., Puig, P., Muñoz, A., Iacono, C. L., Masqué, P., Palanques, A., Acosta J., Guillén J., Ballesteros, M. G., 2016. Morphobathymetric analysis of the large fine-grained sediment waves over the Gulf of Valencia continental slope (NW Mediterranean). Geomorphology. 253, 22-37. https://doi.org/10.1016/j.geomorph.2015.09.027.

Ridente, D., 2018. Late pleistocene post-glacial sea level rise and differential preservation of transgressive "sand ridge" deposits in the Adriatic sea. Geosciences. 8(2), 61. https://doi.org/10.3390/geosciences8020061.

Sabato, L., Tropeano, M., 2004. Fiumara: a kind of high hazard river. Phys. Chem. Earth A/B/C 29(10), 707-715. https://doi.org/10.1016/j.pce.2004.03.008.

Shumaker, L. E., Jobe, Z. R., Graham, S. A., 2017. Evolution of submarine gullies on a prograding slope: Insights from 3D seismic reflection data. Mar. Geol. 393, 35-46. https://doi.org/10.1016/j.margeo.2016.06.006.

Symons, W.O., Sumner, E.J., Talling, P.J., Cartigny, M.J.B., Clare, M.A., 2016. Large-scale sediment waves and scours on the modern seafloor and their implications for the prevalence of supercritical flows. Mar. Geol. 371, 130–148. https://doi.org/10.1016/j.margeo.2015.11.009.

Stich, D., Mancilla, F. D. L., Baumont, D., Morales, J., 2005. Source analysis of the Mw 6.3 2004 Al Hoceima earthquake (Morocco) using regional apparent source time functions. J. Geophys. Res. 110(B6). https://doi.org/10.1029/2004JB003366.

Stich, D., Martín, R., Morales Soto, J., López Comino, J. Á., Mancilla Pérez, F. D. L., 2020. Slip partitioning in the 2016 Alboran Sea earthquake sequence (Western Mediterranean). Front. Earth Sci. 8:587356. https://doi.org/10.3389/feart.2020.587356.

Sultan, N., Cattaneo, A., Urgeles, R., Lee, H., Locat, J., Trincardi, F., Berne S., Canals M., Lafuerza, S., 2008. A geomechanical approach for the genesis of sediment undulations on the Adriatic shelf. Geochem. Geophy. Geosyst. 9(4). https://doi.org/10.1029/2007GC001822.

Tendero-Salmerón, V., Lafosse, M., d'Acremont, E., Rabaute, A., Azzouz, O., Ercilla, G., Makkaoui, M., Galindo-Zaldivar, J., 2021. Application of Automated Throw Backstripping Method to Characterize Recent Faulting Activity Migration in the Al Hoceima Bay (Northeast Morocco): Geodynamic Implications. Front. Earth Sci., 9. https://doi.org/10.3389/feart.2021.645942.

Trincardi, F., Normark, W. R., 1988. Sediment waves on the Tiber prodelta slope: interaction of deltaic sedimentation and currents along the shelf. Geo-Mar Lett. 8(3), 149-157. https://doi.org/10.1007/BF02326091.

Urgeles, R., De Mol, B., Liquete, C., Canals, M., De Batist, M., HughesClarke, J.E., Amblàs, D., Arnau, P.A., Calafat, A.M., Casamor, J.L., Centella, V., De Rycker, K., Fabrés, J., Frigola, J., Lafuerza, S., Lastras, G., Sànchez, A., Zuñiga, D., Versteeg, W., Willmott, V., 2007. Sediments undulations on the Llobregat prodelta: signs of early slope instability or sedimentary bedforms? J. Geophys. Res. 112, B05102. https://doi.org/10.1007/s11001-011-9125-1.

Urgeles, R., Cattaneo, A., Puig, P., Liquete, C., De Mol, B., Amblàs, D., Sultan N., Trincardi, F., 2011. A review of undulated sediment features on Mediterranean prodeltas: distinguishing sediment transport

structures from sediment deformation. Mar. Geophys. Res. 32(1-2), 49-69. https://doi.org/10.1007/s11001-011-9125-1.

van Haren, H., Puig, P., 2017. Internal wave turbulence in the Llobregat prodelta (NW Mediterranean) under stratified conditions: A mechanism for sediment waves generation?. Mar. Geol. 388, 1-11. https://doi.org/10.1016/j.margeo.2017.04.008.

Viúdez, A., Pinot, J. M., Haney, R. L., 1998. On the upper layer circulation in the Alboran Sea. J. Geophys. Res. 103(C10), 21653-21666. https://doi.org/10.1029/98JC01082.

Westaway, R., 1993. Quaternary uplift of southern Italy. J. Geophys. Res. *98*(B12), 21741-21772. https://doi.org/10.1029/93JB01566.

Wynn, R. B., Stow, D. A., 2002. Classification and characterisation of deep-water sediment waves. Mar. Geol. 192(1-3), 7-22. https://doi.org/10.1016/S0025-3227(02)00547-9.

Table 1. Main hydrographical, hydrological, and sedimentological features of the Mazzarrà and Rhis-Nekor rivers. The estimated values were computed using equations 1 and 2 of Milliman and Syvitski (1992). The "b" value was obtained using equation 4 of Syvitski et al. (2000) (see Appendix SM1 in supplementary material). Missing values (-) mean no available data.

River	Mazzarrà	Nekor	Rhis
Basin area (km^2)	119.23	854	836
Maximum basin elevation (m)	1288	2000	2000
Maximum river elevation (m)	1204	1300	1180
River length (km)	24.54	82.06	77.8
River slope (degree)	4.91	1.59	1.51
Delta area (km^2)	15	30	30
Mean precipitation (mm yr^{-1})	770	340	-
Mean annual temperature (°C)	17	18.1	18.1
Mean annual discharge (m^3 s^{-1})	-	2.17	-
Historical maximum discharge (m^3 s^{-1})	500 - 777	-	-
Potential sediment load (Kg s^{-1})	-	113.33	-
Estimated potential sediment load (Kg s^{-1})	2.2	138.7	137.1
Mean sediment yield (t km^2 yr^{-1})	-	4967	-
Estimated mean sediment yield (t km^2 yr^{-1})	847.5	5416.9	5470.2
b	-	0.841	-

Table 2. Main morphometric parameters of the sediment undulations in the Mazzarrà and Rhis-Nekor prodeltas. Similar parameters reported in the literature for other Mediterranean and extra-Mediterranean prodeltas are listed. Missing values (-) mean no data available. * prodelta in a lake setting.

Sediment undulations in the Mazzarrà prodelta							
	Wave height (m)	Wave length (m)	*H/L* index	Lateral length (m)	Asymmetry	Slope (°)	
Minimum	0.05	16	0.001	30	-0.81	0.46	
Maximum	4.4	242	0.032	1309.6	0.62	2.75	
Mean	0.77	74.2	0.007	220.2	-0.007	1.43	
Std. deviation	0.61	68.9	0.006	167.5	0.001	1.41	
Count	596	596	596	596	596	596	
Sediment undulations in the Rhis-Nekor prodelta							
Minimum	0.04	40	0.001	22	-0.73	0.11	
Maximum	2.33	456	0.015	3043.1	0.68	1.99	
Mean	0.8	141.6	0.004	312	0.008	0.86	
Std. deviation	0.5	60.3	0.001	325	0.22	0.3	
Count	510	510	510	510	510	510	
Sediment undulations in other Mediterranean prodeltas							
Adra	0.04 - 2.34 (0.45)	21 - 244 (76)	~ 0.003 (0.006)	-	-	3.1	Bárcenas et al. (2009)
Central Adriatic	0.17 – 3.76 (0.92)	53 – 477 (212)	0.01 -0.0025 (0.004)	-	-	0.2 - 1	Cattaneo et al. (2004)
Albunol	0.02 – 4.22 (0.53)	23 – 163 (61)	0.003 (0.008)	-	-	4.5	Bárcenas et al. (2009)
Ebro	0.2 – 2 (1.1)	145 – 320 (222)	0.01 - 0.002 (0.005)	480 – 1300	-	1	Urgeles et al. (2011)
Fluvià-Muga	0.5 – 4	~ 1000	-	100 – 1000	-	0.6	Urgeles et al. (2011)
Guadalfeo	0.07 – 5 (0.85)	19 – 252 (80)	0.007 (0.01)	30.4 – 1989 (210.8)	-	1.1	Fernández-Salas et al. (2007)
Gualchos	0.002 – 2.21 (0.32)	19 – 142 (53)	~ 0.003 (0.006)	-	-	3.7	Bárcenas et al. (2009)
Gulf of Corinth and Kyparissiakos	-	80 - 150	-	-	-	0.5 - 2	Lykousis et al. (2009)
Llobregat	0.03 – 1.3 (0.55)	37 – 235 (105)	0.01 – 0.002 (0.005)	300 - 2000	-	0.3 – 3 (2)	Urgeles et al. (2007)
Seco	0.06 – 2.19 (0.70)	25 – 74 (46)	0.006 (0.015)	-	-	4	Bárcenas et al. (2009)
Verde	0.13 – 1.28 (1.05)	38 – 103 (73)	0.005 (0.01)	-	-	5	Bárcenas et al. (2009)
Tiber	7 (max)	~ 100	-	-	-	0.7 – 1.2	Urgeles et al. (2011)
Sediment undulations in other prodeltas (worldwide)							
Fraser	1 - 3	20 - 150	0.15 – 0.006	-	-	1 - 3 (1.5)	Hill (2012)
Squamish	~1.5	30 – 40	0.05 – 0.03	-	-	~ 6	Hughes Clarke et al.

							(2012)
Noeick	~5	50 - 100	0.1 – 0.05	-	-	4 - 5	Bornhold and Prior (1990)
Rhone*	0.5 – 2	30 - 100	0.005 – 0.06	-	-	-	Girardclos et al. (2012)

Table 3. Spearman correlation coefficients from principal component analysis. The highlighted values are the strongly positively and negatively correlated (values above 0.5). *Asym*: Asymmetry, *H*: Wave height, *L*: Wave length, Llength: Lateral length, Depth: Water depth, Slope: Basal slope of undulations, Distance: Distance from the river mouth, HST: Thickness of highstand systems tract.

PC	Variance Explained (%)	*Asym*	Log *H*	Log *L*	Llength	Depth	Slope	Distance	HST
1	37.20	-0.07	0.19	0.45	0.44	-0.38	**-0.76**	**0.95**	**-0.86**
2	23.25	0.15	**0.86**	**0.75**	0.45	0.34	0.40	-0.06	-0.02
3	13.12	**0.73**	0.17	-0.18	0.07	**-0.58**	0.29	-0.06	-0.02
4	12.31	**0.59**	-0.20	0.22	-0.34	**-0.5**[illegible]	-0.20	0.18	-0.16
5	7.95	0.23	-0.25	-0.21	0.41	0.[illegible]1	-0.10	-0.11	0.22
6	2.75	-0.01	-0.20	0.24	-0.01	-0.[illegible]	0.26	0.07	-0.18
7	1.84	0.03	-0.10	0.14	-0.07	-0.12	-0.12	0.06	0.26
8	1.47	-0.02	0.07	-0.08	-0.06	0.05	0.05	0.28	-0.03

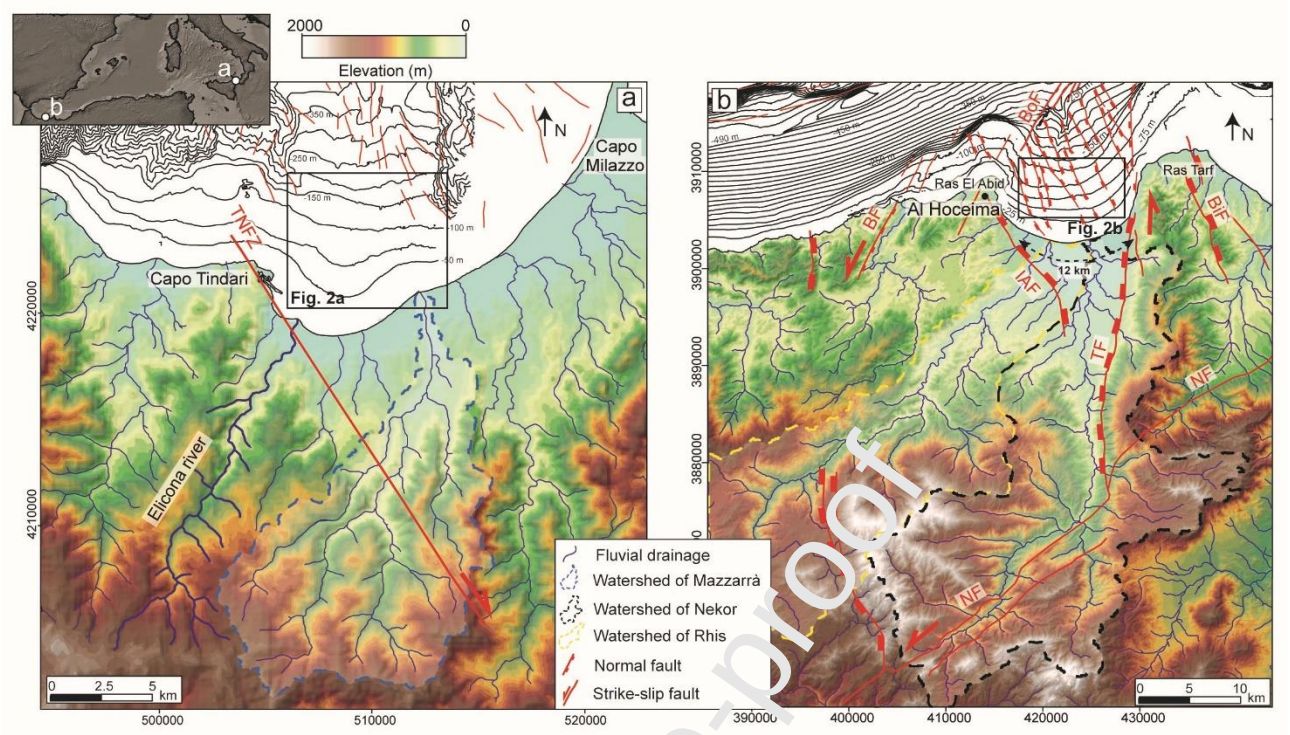

Figure 1. a) Topography and isobaths in the Gulf of Patti. The red lines indicate the main faults (from Cultrera et al., 2016); TNFZ : Tindari-Rocca Novara fault zone. The box in the inset indicates the location of the two study areas. b) Topography and isobaths in Al-Hoceima Bay. The red lines indicate the main faults (from Lafosse et al., 2017): BiF: Boudinar fault; IAF: Ajdir-Imzouren fault; TF: Trougout fault; NF: Nekor fault; BF: Boussekour fault; BoF: Bokkoya fault. The topography is extracted from the ASTER GDEM (http://gdem.ersdac.jspacesystems.or.jp/).

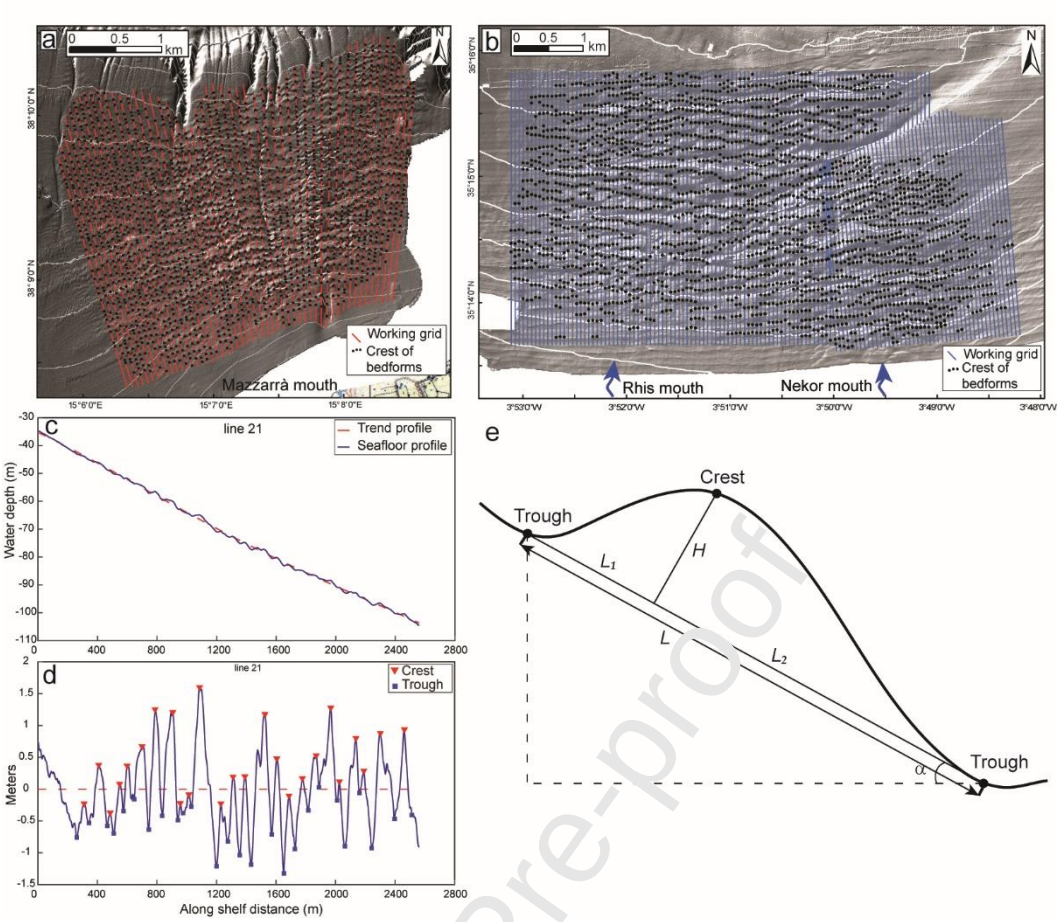

Figure 2. Morphometric characterization of sediment undulations in the two study areas. a) Grid of bathymetric profiles in the Mazzarrà prodelta. b) Grid of bathymetric profiles in Rhis-Nekor prodelta. c) Bathymetric profile in blue and the related best-fit curve in red. d) Detrending of bathymetric profiles using the best-fit curve (the elevation of the undulations is shown). e) Scheme of the morphometric parameters measured for undulations: *H:* wave height, *L:* wave length, $L_{1:}$ upslope length, $L_{2:}$ downslope length, α: basal slope of undulations.

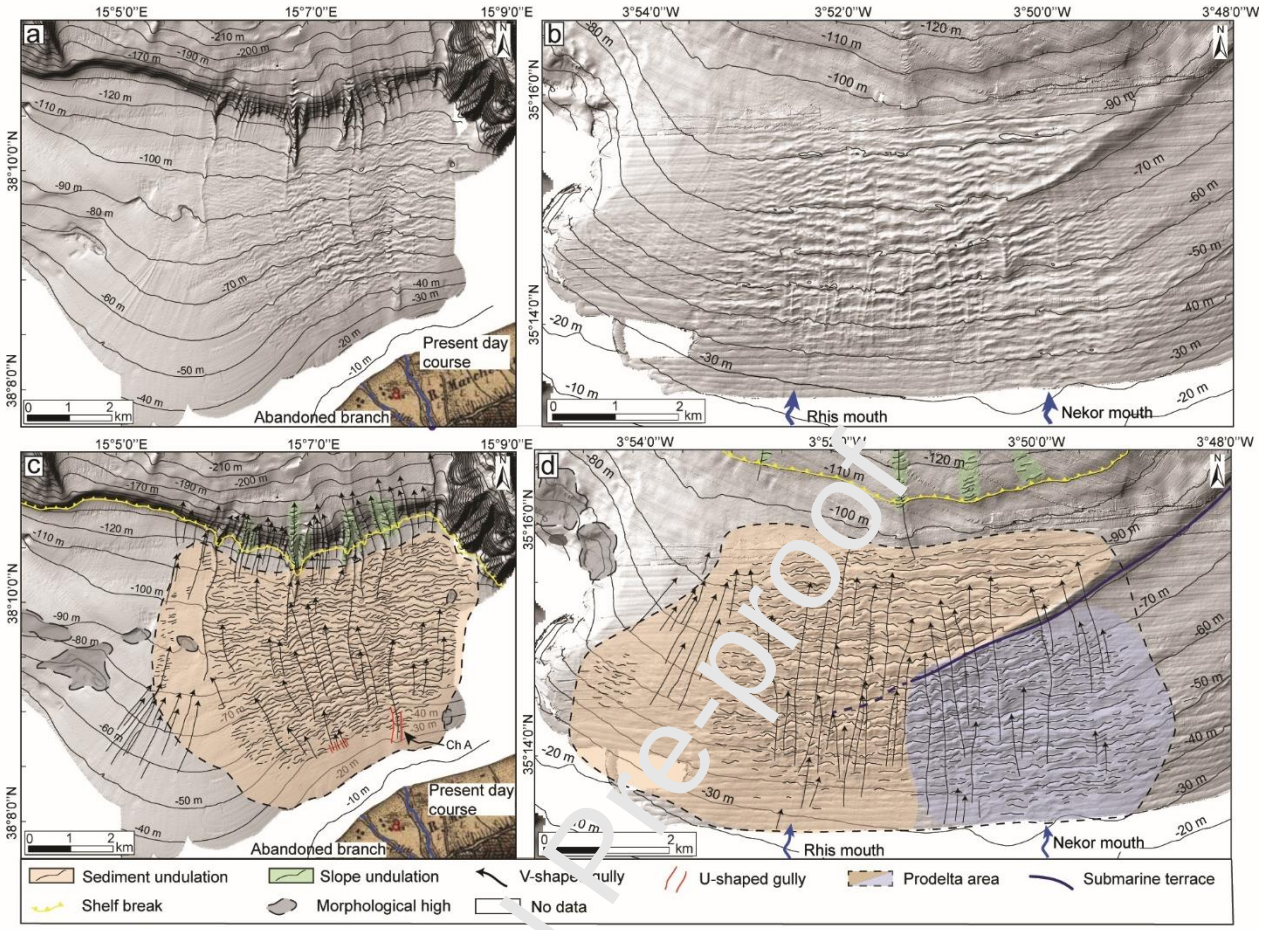

Figure 3. Multibeam morpho-bathymetry (shaded relief) of the two study areas (a-b) and morphological interpretation (c-d). The Mazzarrà prodelta area is on the left (a, c; location in fig. 1); the Rhis-Nekor prodelta area is on the right (b, d; location in Fig. 1).

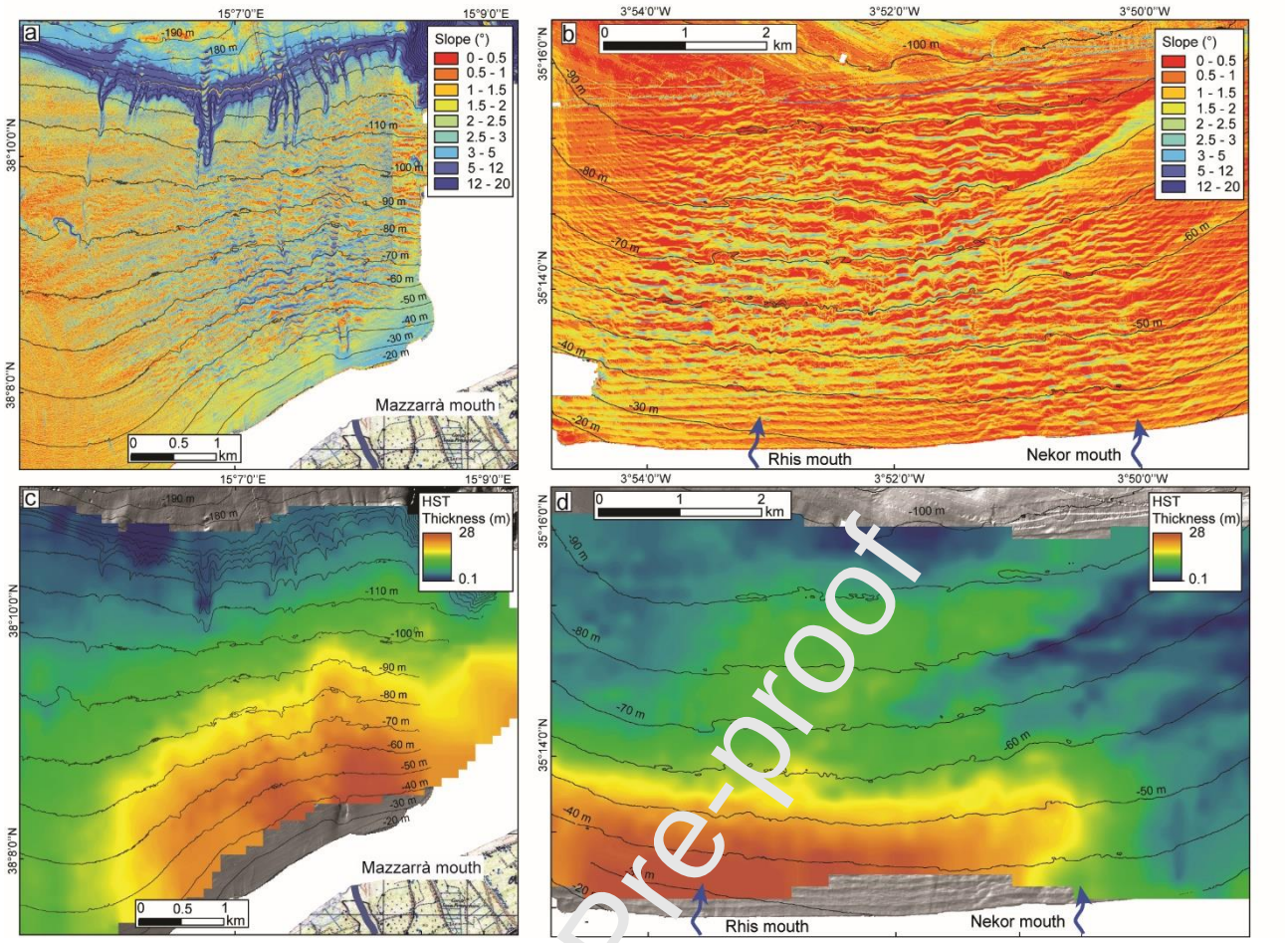

Figure 4. Slope gradient map of the two study areas (a: Mazzarrà prodelta; b: Rhis-Nekor prodelta). Thickness distribution of the Late Holocene highstand systems tract (c: Mazzarrà prodelta; d: Rhis-Nekor prodelta).

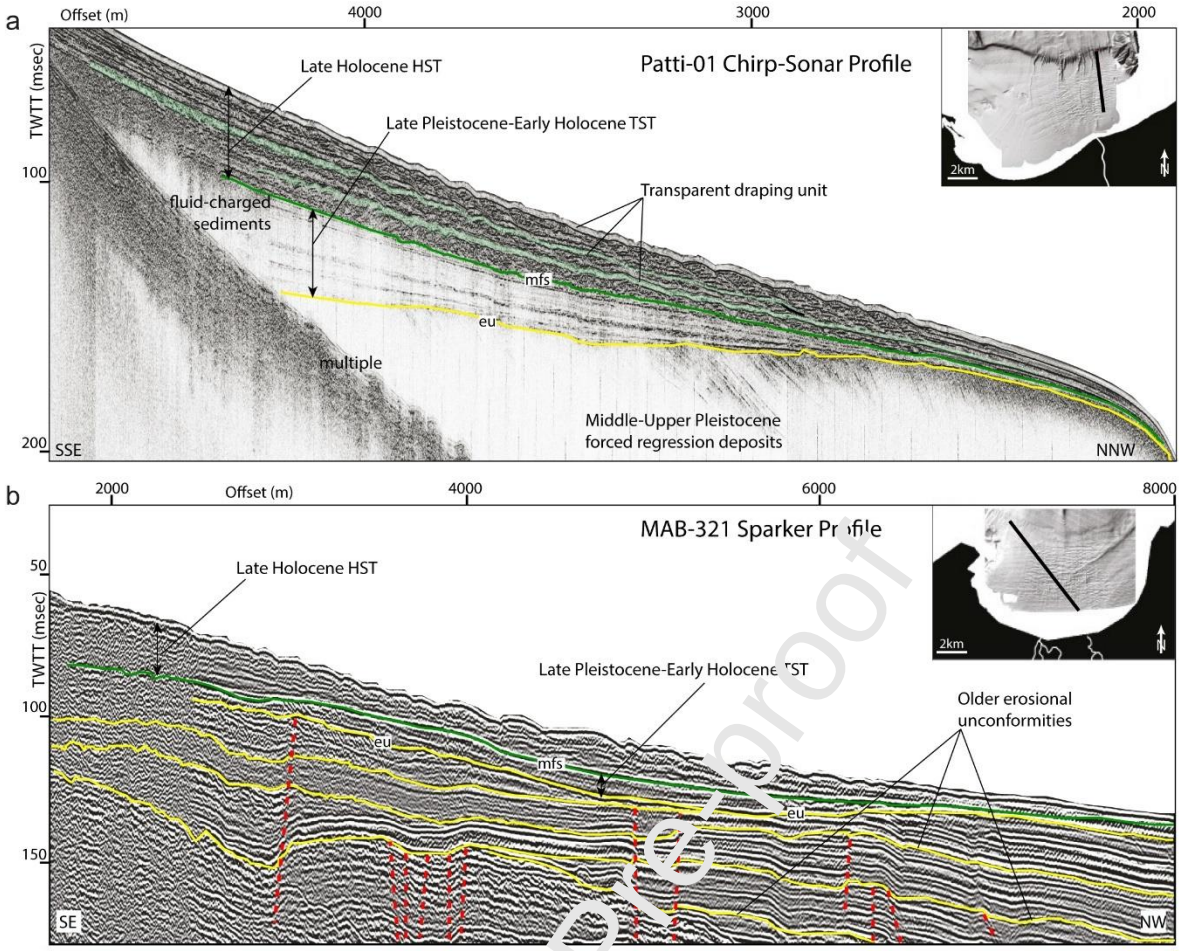

Figure 5. Along-slope seismic profile across the shelf of Gulf of Patti (a) and A-Hoceima Bay (b). Note the presence of an undulated pattern only in the uppermost prograding units (Late Holocene HST) in both the prodelta deposits. msf : maximum flooding surface, eu : erosional unconformity, dashed red lines : faults, TWTT : Two-Way Travel Time.

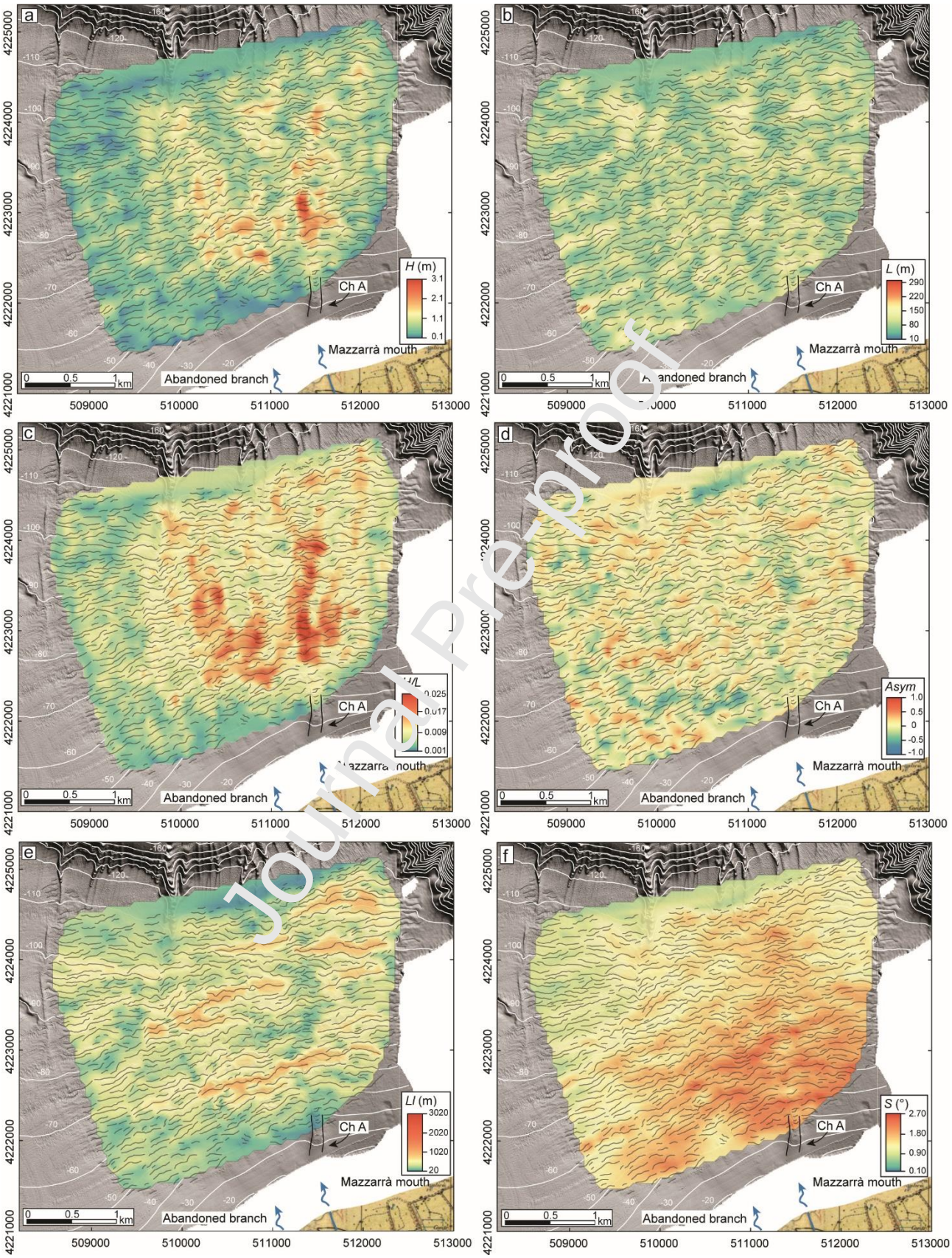

Figure 6. Spatial distribution of morphometric parameters of undulations in the Mazzarrà prodelta. a) *H*: Wave height, b) *L*: Wave length, c) *H/L*: Aspect ratio, d) *Asym*: Asymmetry, e) *Ll*: Lateral length, f) *S*: Basal slope of undulations. ChA is the largest U-shaped incision facing the modern Mazzarrà River mouth.

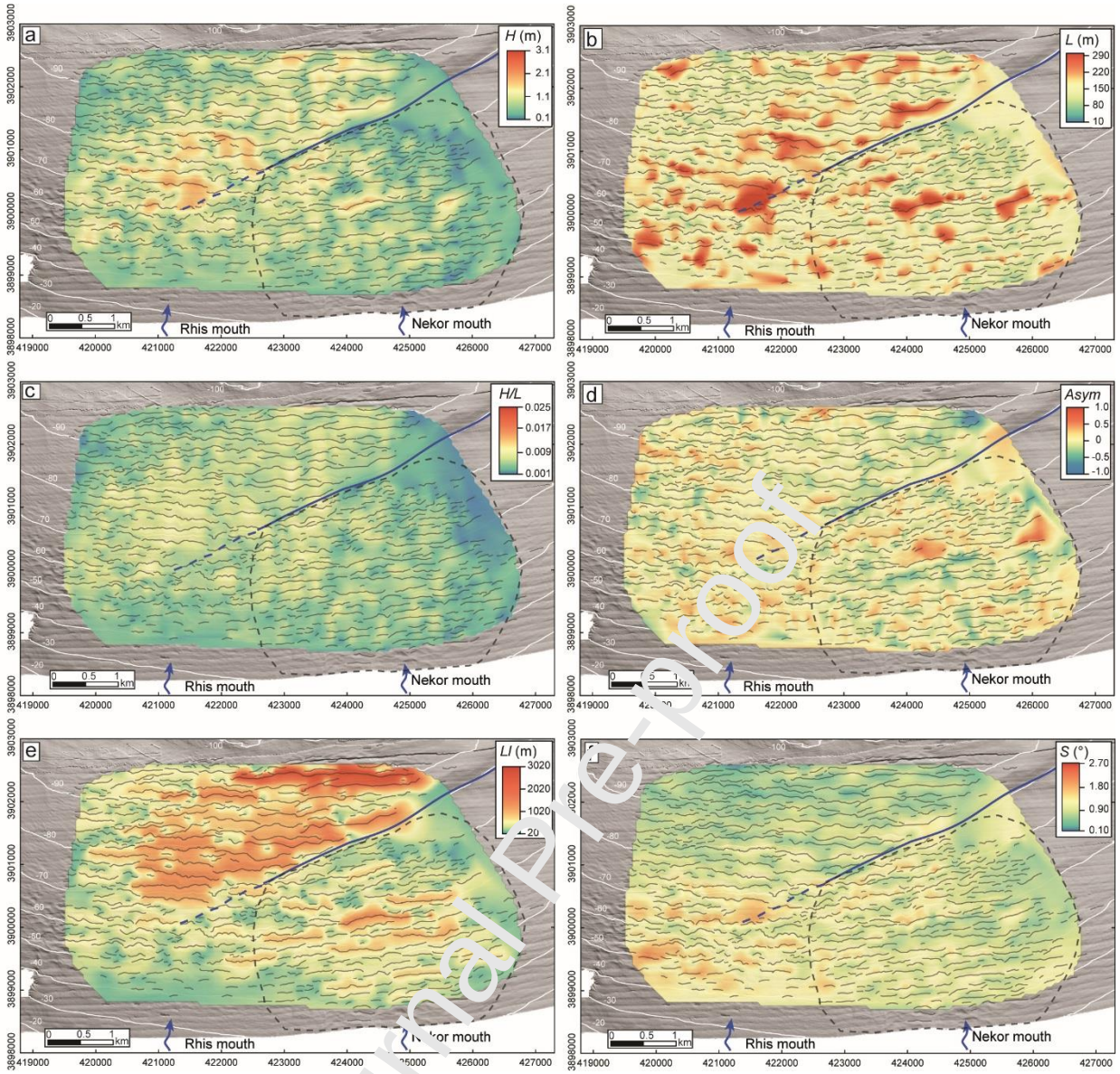

Figure 7. Spatial distribution of morphometric parameters of undulations in the Rhis-Nekor prodelta. a) *H*: Wave height, b) *L*: Wave length, c) *H/L*: Aspect ratio, d) *Asym*: Asymmetry, e) *Ll*: Lateral length, f) *S*: Basal slope of undulations. The blue line marks the position of the submarine terrace, the dashed part marks its buried continuation (Lafosse et al., 2018). The black dashed polygon indicates the prodelta sector facing the Nekor River mouth.

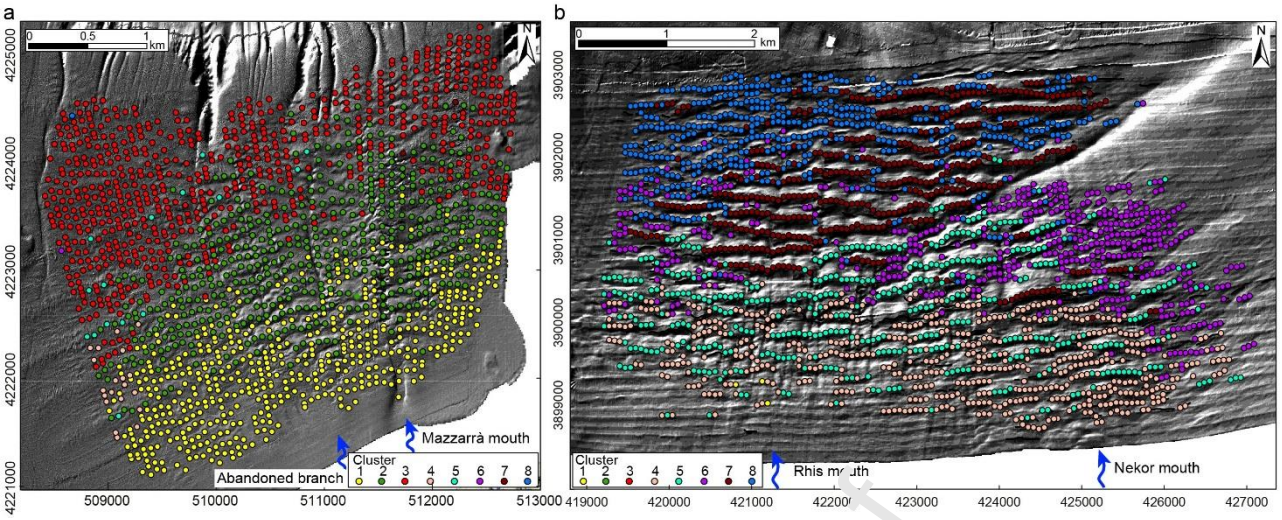

Figure 8. a) Distribution of the clusters of sedim

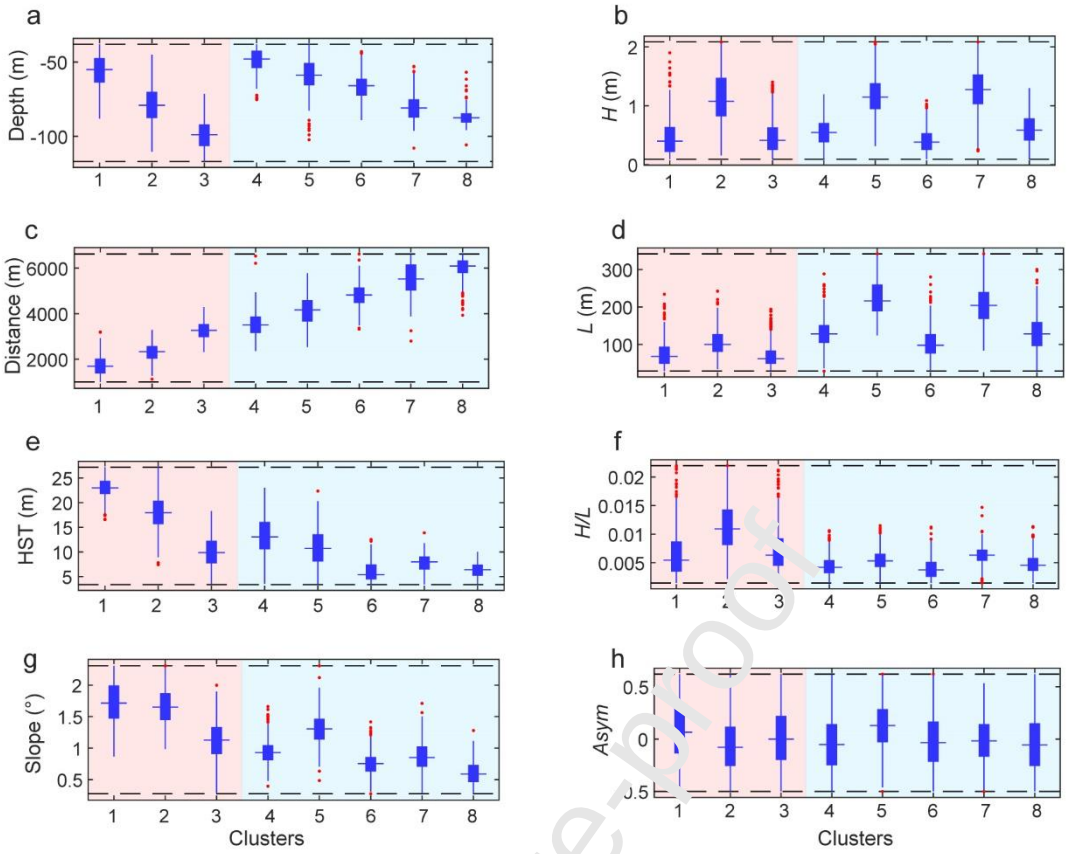

Figure 9. Boxplot of the main morphometric parameters and comparison with local factors that may control their distribution. Pink refers to the Mazzarrà prodelta; pale blue to the Rhis-Nekor prodelta. Slope: Basal slope, Distance: Distance from the river mouth, HST: Highstand thickness, *H*: Wave height, *L*: Wavelength, *H/L*: Aspect ratio, *Asym*: Asymmetry. Boxplot components: central tendency is median (Q2), limits of box are interquartile range (IQR) from 25% (Q1, lower boundary) to 75% (Q3, higher boundary) of the data, the limits of the line are Q1-(1.5 x IQR) and Q3+(1.5 x IQR). The red dots represent the outliers.

Figure 10. Time lapse aerial images of river mouths (aerial photos from Google Earth). a, b) Time lapse aerial images (2015–2018) of the present-day Rhis mouth. c, d) Time lapse aerial images (2011-2012) of the present-day mouth of Nekor River. e, f) Time lapse aerial images (2012- 2014) of the present-day mouth of Mazzarrà River. Red dashed line is the coastal line after flash-flood event.

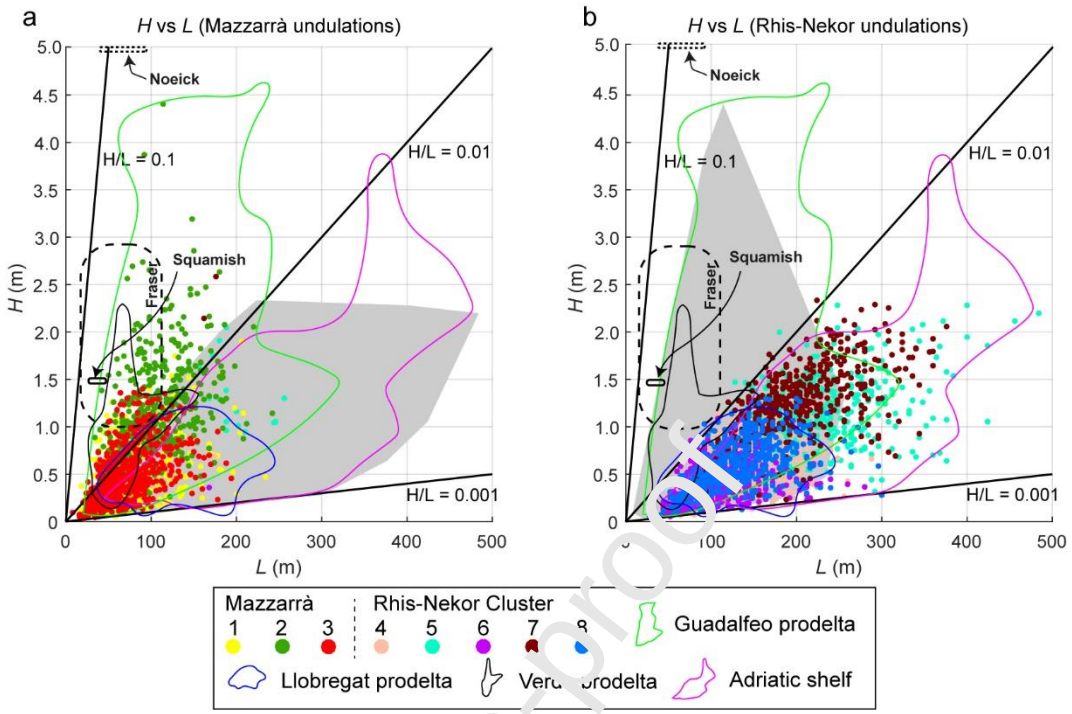

Figure 11. Scatterplot of wave height (*H*) vs wavelength (*L*) of sediment undulations in the two study areas and in other Mediterranean locations. Grey areas indicate the extent of the datapoints. Colored dots correspond to the different clusters (1 to 8). References linked with Mediterranean and extra-Mediterranean fields of sediment waves are reported in Table 2.

Highlights:

Genesis of coexisting depositional and erosional bedforms in prodelta settings
Quantitative and statistical analysis to unveil the mechanism behind the bedforms
Controlling factors of the sedimentary gravity flows and associated bedforms

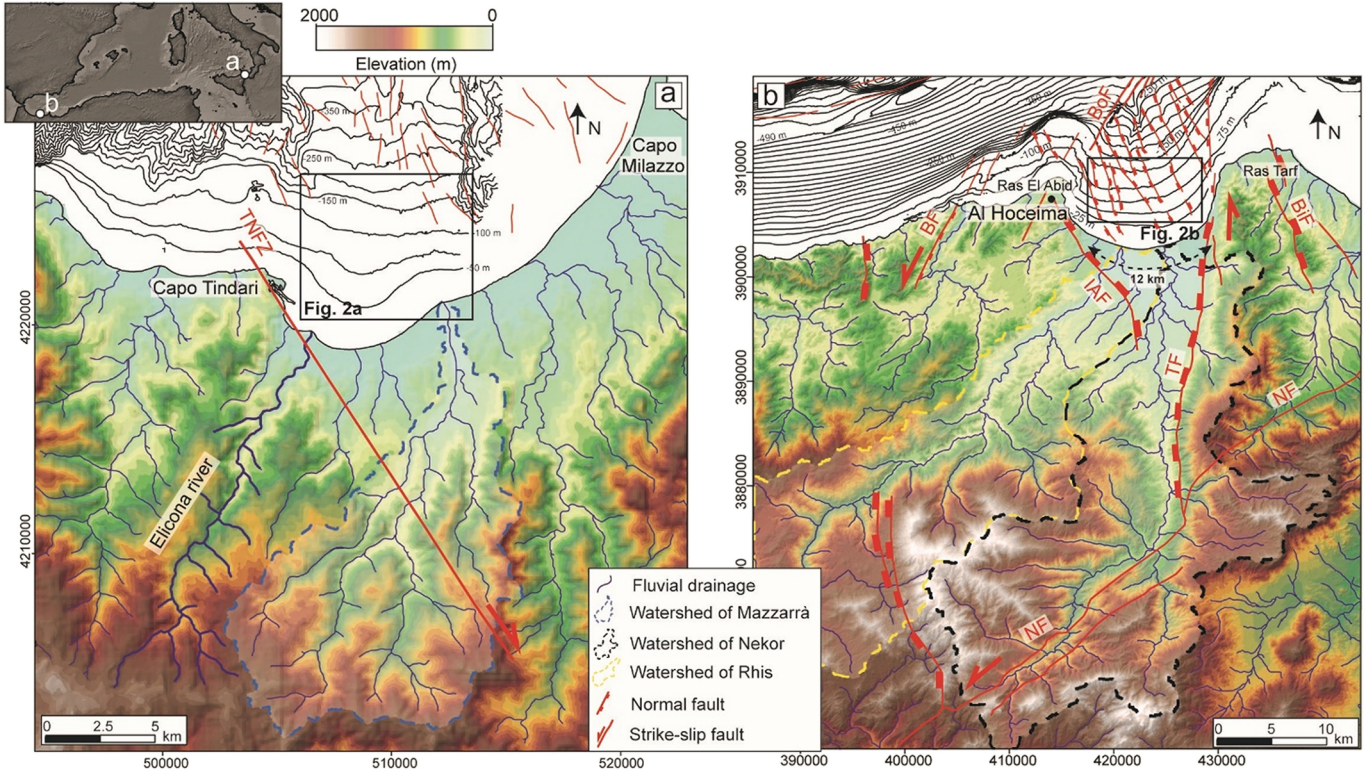
2000
0
Elevation (m)
a
b
N
Capo Milazzo
Capo Tindari
TNFZ
Fig. 2a
Elicona river
Fluvial drainage
Watershed of Mazzarrà
Watershed of Nekor
Watershed of Rhis
Normal fault
Strike-slip fault
0 2.5 5 km
4220000
4210000
500000
510000
520000
b
Ras El Abid
Al Hoceima
Fig. 2b
BoF
BF
IAF
TF
NF
Ras Tarf
12 km
0 5 10 km
3910000
3900000
3890000
3880000
390000
400000
410000
420000
430000

Figure 1

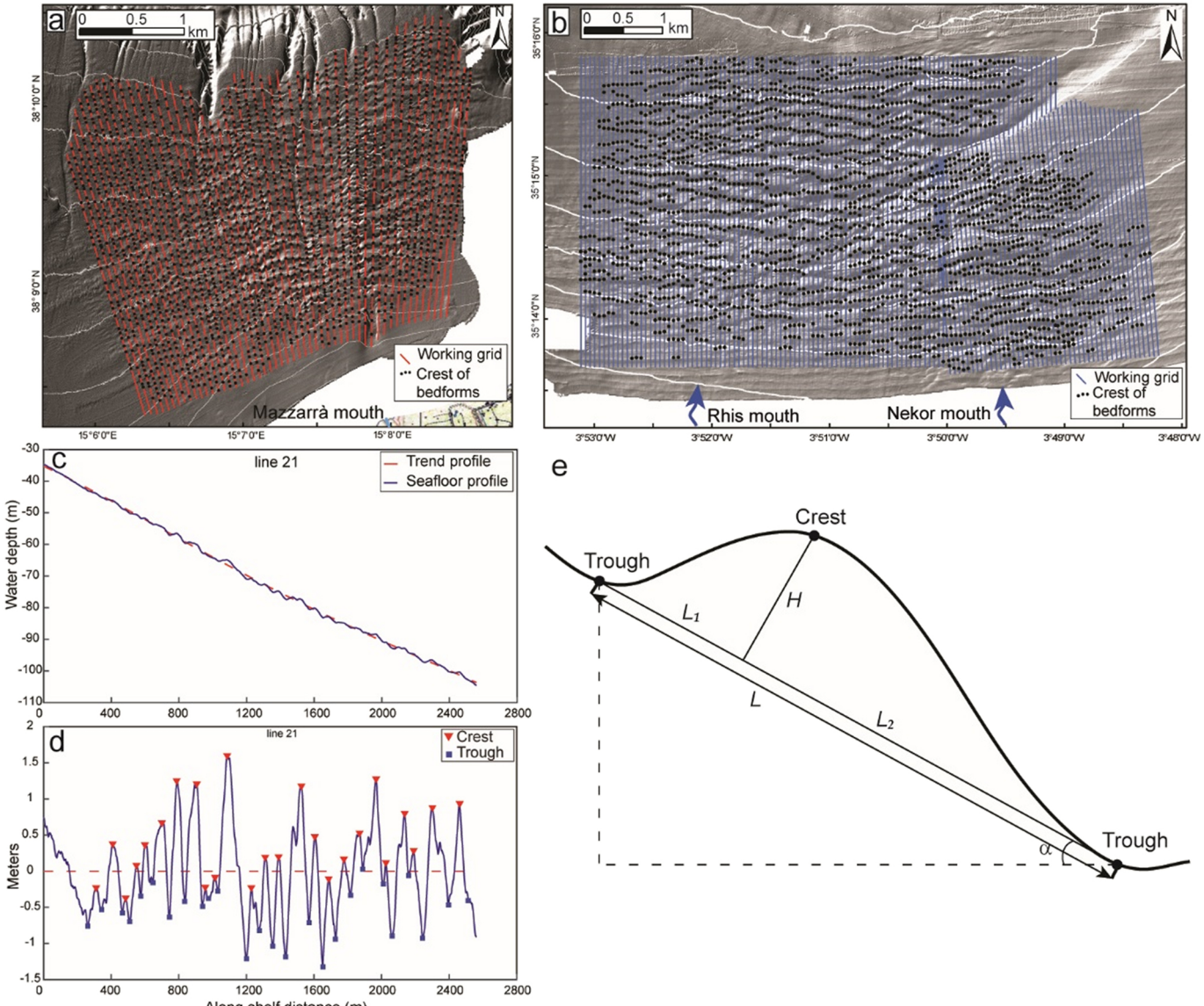
a
0 0.5 1 km
N
38°10'0"N
38°9'0"N
15°6'0"E
15°7'0"E
15°8'0"E
Working grid
Crest of bedforms
Mazzarrà mouth
b
0 0.5 1 km
N
35°16'0"N
35°15'0"N
35°14'0"N
3°53'0"W
3°52'0"W
3°51'0"W
3°50'0"W
3°49'0"W
3°48'0"W
Working grid
Crest of bedforms
Rhis mouth
Nekor mouth
c
line 21
Trend profile
Seafloor profile
Water depth (m)
d
line 21
Crest
Trough
Meters
Along shelf distance (m)
e
Crest
Trough
Trough
H
L1
L
L2
α

Figure 2

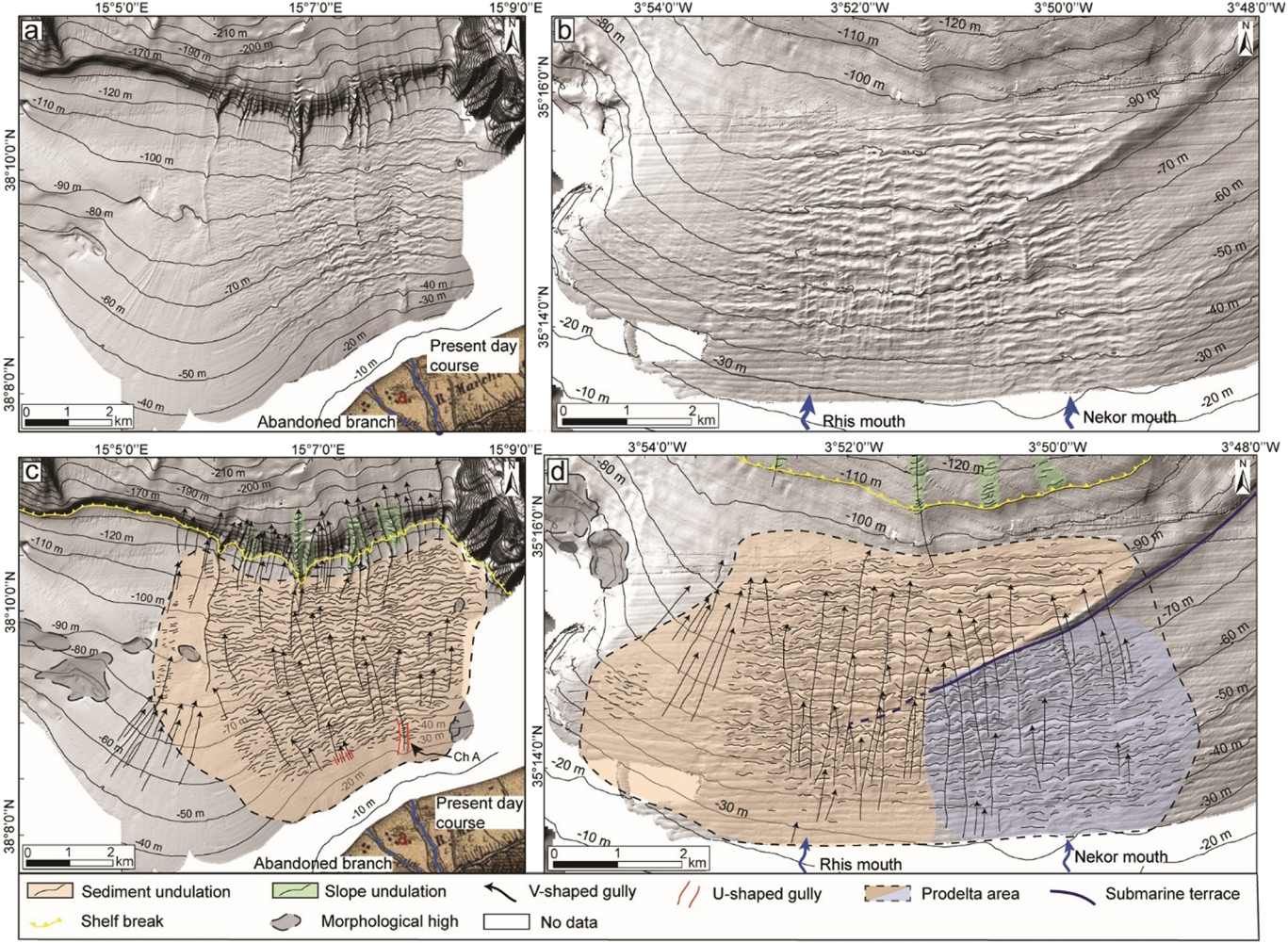
a
b
c
d
15°5'0"E
15°7'0"E
15°9'0"E
3°54'0"W
3°52'0"W
3°50'0"W
3°48'0"W
38°10'0"N
38°8'0"N
35°16'0"N
35°14'0"N
N
-210 m
-200 m
-190 m
-170 m
-120 m
-110 m
-100 m
-90 m
-80 m
-70 m
-60 m
-50 m
-40 m
-30 m
-20 m
-10 m
Present day course
Abandoned branch
Rhis mouth
Nekor mouth
Ch A
0 1 2 km
Sediment undulation
Slope undulation
V-shaped gully
U-shaped gully
Prodelta area
Submarine terrace
Shelf break
Morphological high
No data

Figure 3

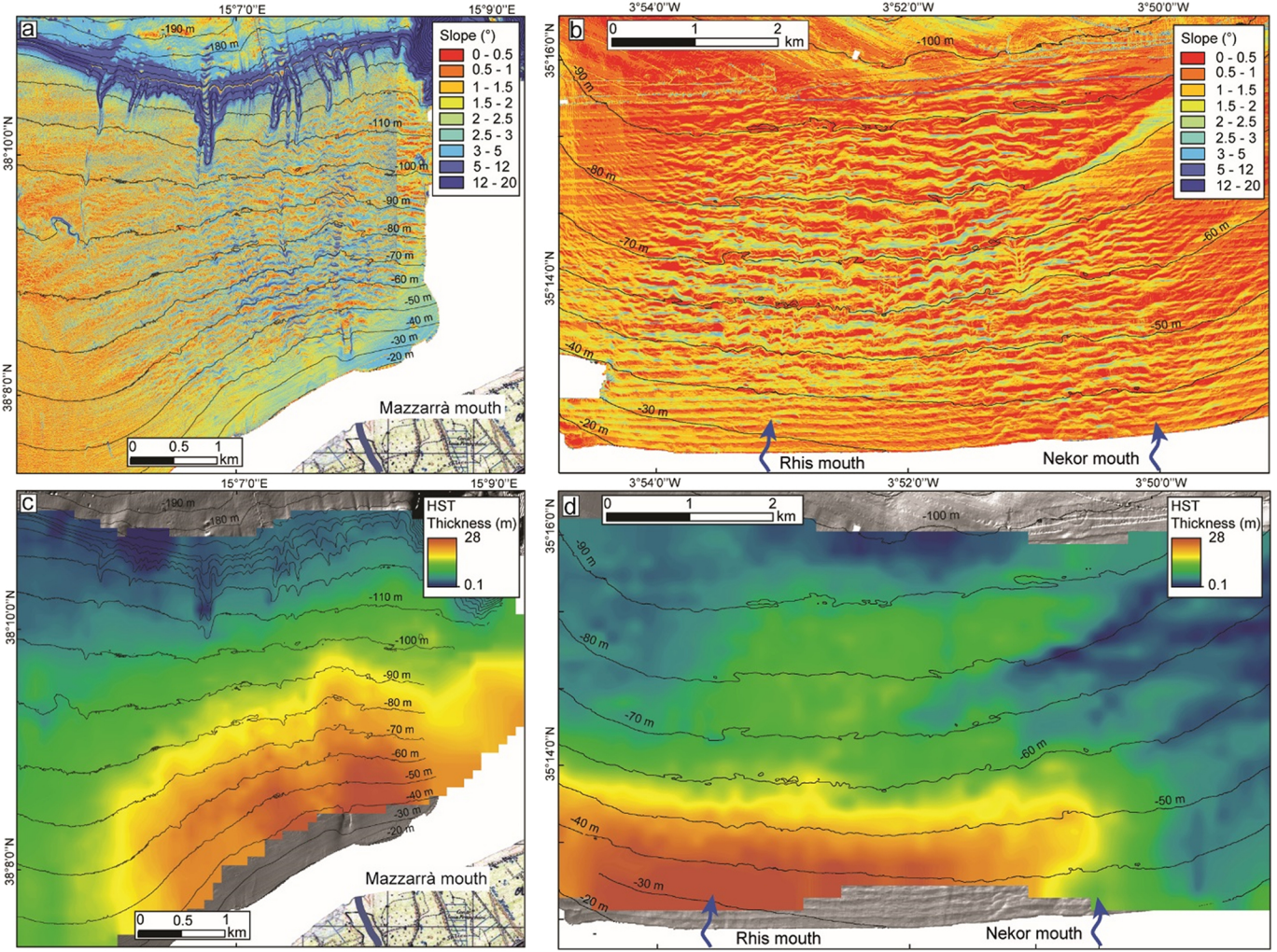
a
15°7'0"E
15°9'0"E
38°10'0"N
38°8'0"N
Slope (°)
0 - 0.5
0.5 - 1
1 - 1.5
1.5 - 2
2 - 2.5
2.5 - 3
3 - 5
5 - 12
12 - 20
-190 m
-180 m
-110 m
-100 m
-90 m
-80 m
-70 m
-60 m
-50 m
-40 m
-30 m
-20 m
Mazzarrà mouth
0 0.5 1 km
b
3°54'0"W
3°52'0"W
3°50'0"W
35°16'0"N
35°14'0"N
0 1 2 km
Slope (°)
0 - 0.5
0.5 - 1
1 - 1.5
1.5 - 2
2 - 2.5
2.5 - 3
3 - 5
5 - 12
12 - 20
-100 m
-90 m
-80 m
-70 m
-60 m
-50 m
-40 m
-30 m
-20 m
Rhis mouth
Nekor mouth
c
15°7'0"E
15°9'0"E
38°10'0"N
38°8'0"N
HST
Thickness (m)
28
0.1
-190 m
-180 m
-110 m
-100 m
-90 m
-80 m
-70 m
-60 m
-50 m
-40 m
-30 m
-20 m
Mazzarrà mouth
0 0.5 1 km
d
3°54'0"W
3°52'0"W
3°50'0"W
35°16'0"N
35°14'0"N
0 1 2 km
HST
Thickness (m)
28
0.1
-100 m
-90 m
-80 m
-70 m
-60 m
-50 m
-40 m
-30 m
-20 m
Rhis mouth
Nekor mouth

Figure 4

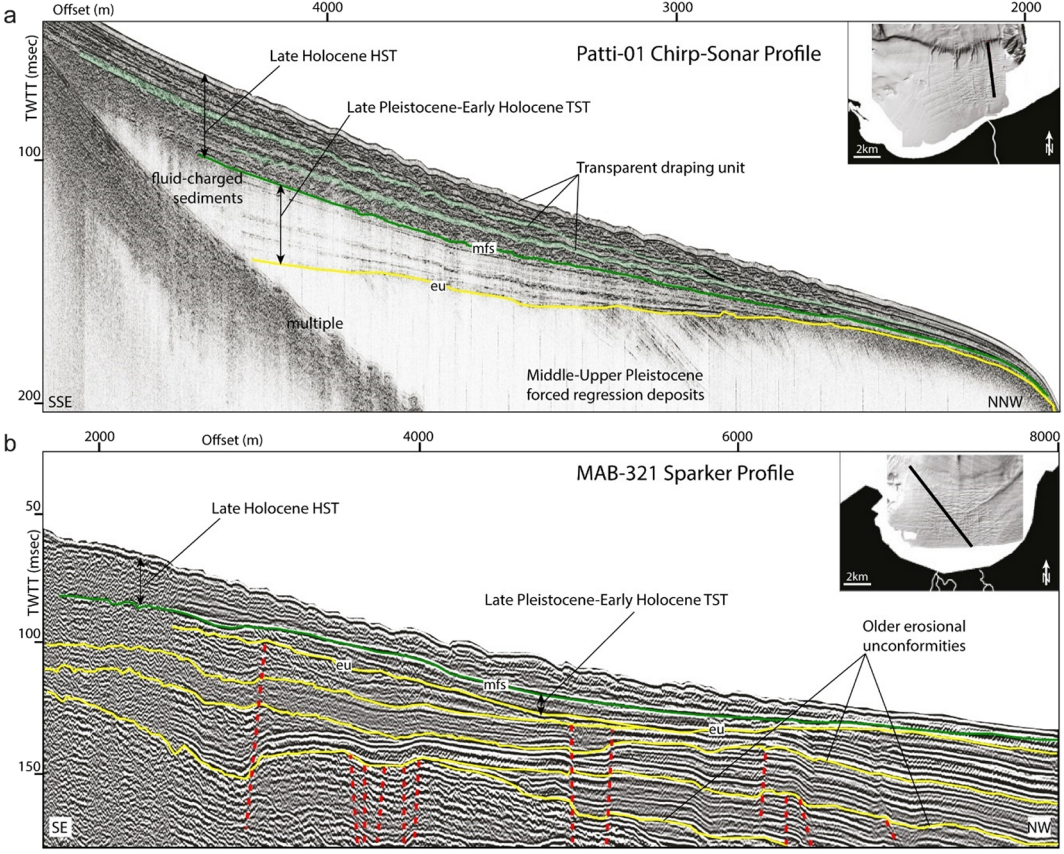
a
Offset (m)
4000
3000
2000
TWTT (msec)
100
200
Patti-01 Chirp-Sonar Profile
Late Holocene HST
Late Pleistocene-Early Holocene TST
Transparent draping unit
fluid-charged sediments
mfs
eu
multiple
Middle-Upper Pleistocene forced regression deposits
SSE
NNW
2km
b
2000
Offset (m)
4000
6000
8000
50
TWTT (msec)
100
150
MAB-321 Sparker Profile
Late Holocene HST
Late Pleistocene-Early Holocene TST
Older erosional unconformities
eu
mfs
eu
SE
NW
2km

Figure 5

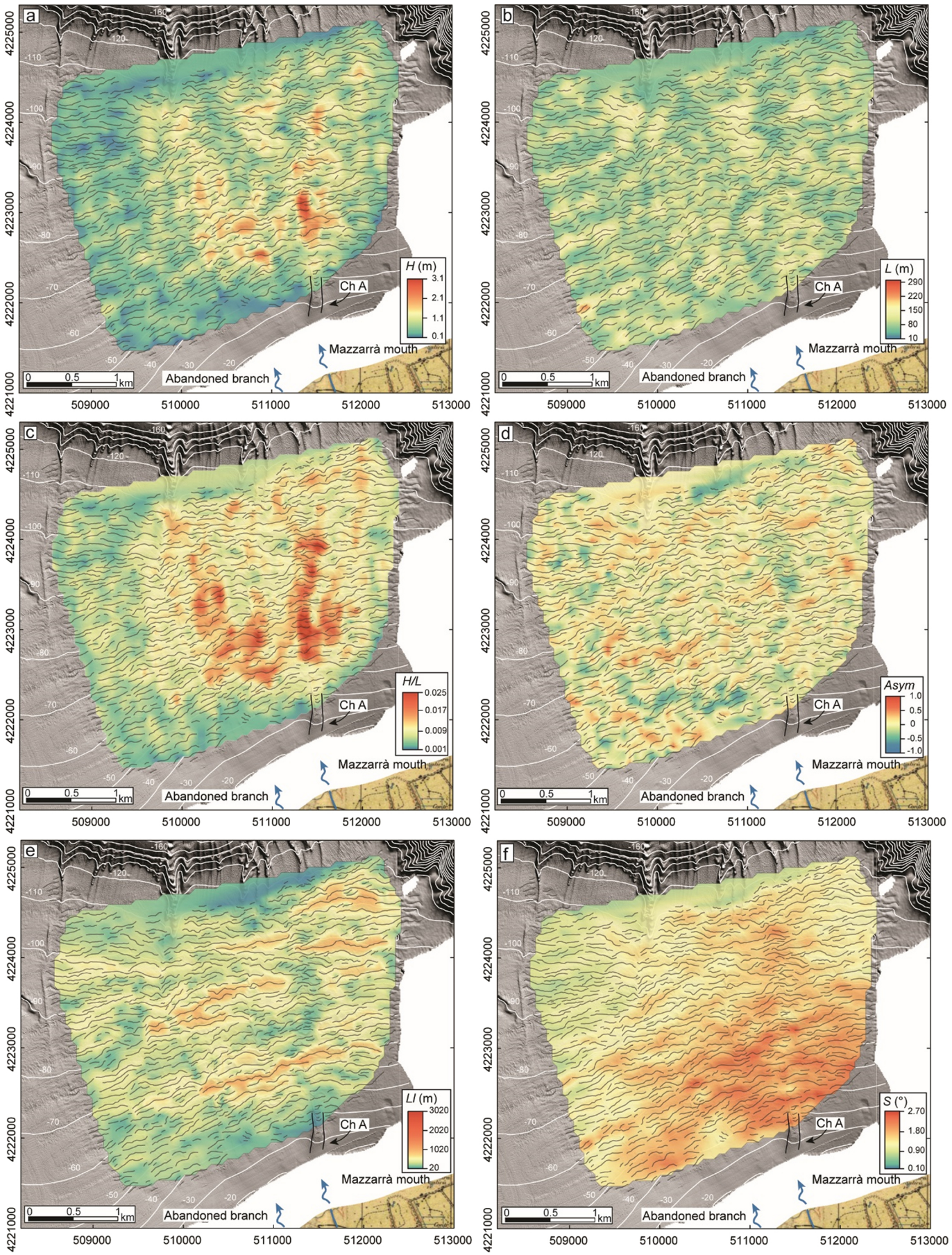
a
H (m)
3.1
2.1
1.1
0.1
b
L (m)
290
220
150
80
10
c
H/L
0.025
0.017
0.009
0.001
d
Asym
1.0
0.5
0
-0.5
-1.0
e
LI (m)
3020
2020
1020
20
f
S (°)
2.70
1.80
0.90
0.10
Ch A
Mazzarrà mouth
Abandoned branch
0 0.5 1 km
4225000
4224000
4223000
4222000
4221000
509000
510000
511000
512000
513000

Figure 6

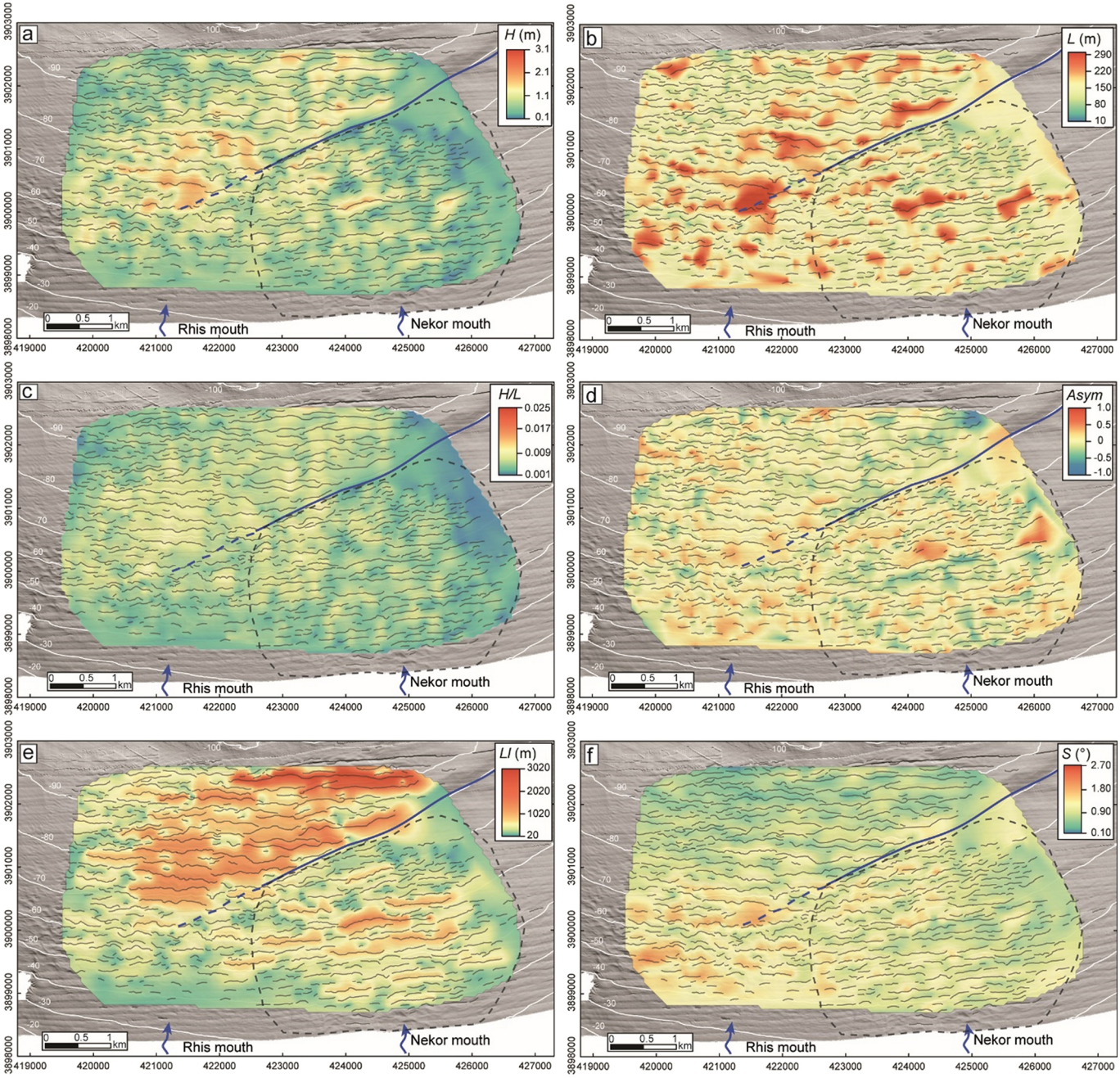
a
H (m)
3.1
2.1
1.1
0.1
b
L (m)
290
220
150
80
10
c
H/L
0.025
0.017
0.009
0.001
d
Asym
1.0
0.5
0
-0.5
-1.0
e
LI (m)
3020
2020
1020
20
f
S (°)
2.70
1.80
0.90
0.10
0 0.5 1 km
Rhis mouth
Nekor mouth
419000
420000
421000
422000
423000
424000
425000
426000
427000
3898000
3899000
3900000
3901000
3902000
3903000

Figure 7

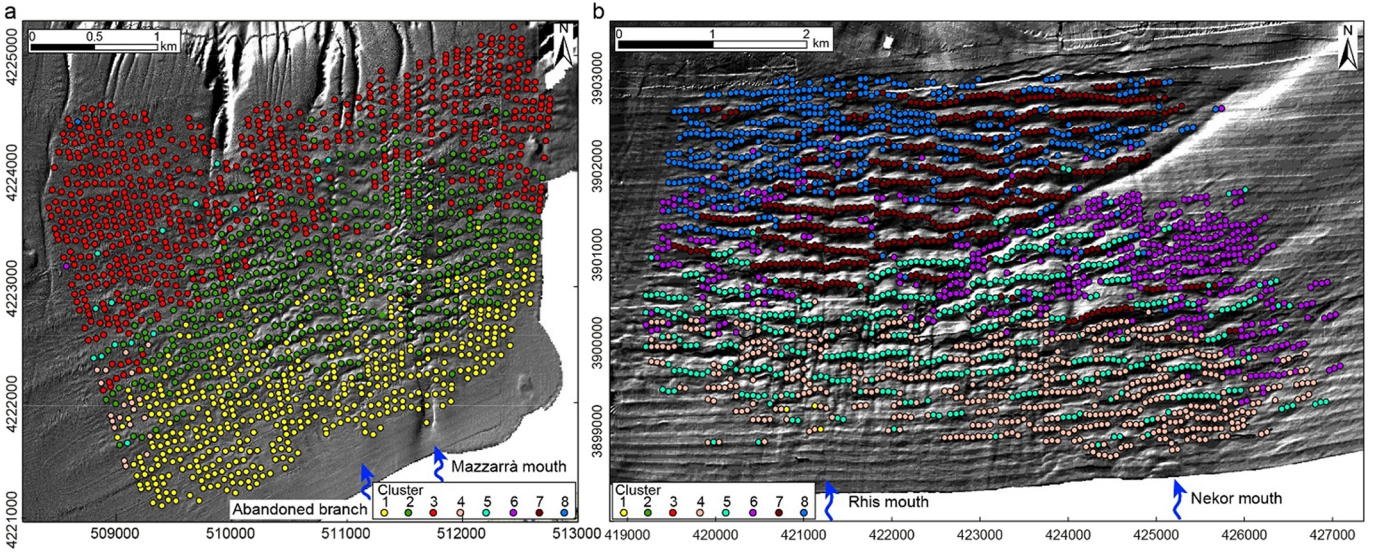
a
0 0.5 1 km
N
Mazzarrà mouth
Abandoned branch
Cluster
1 2 3 4 5 6 7 8
4225000
4224000
4223000
4222000
4221000
509000
510000
511000
512000
513000
b
0 1 2 km
N
Rhis mouth
Nekor mouth
Cluster
1 2 3 4 5 6 7 8
3903000
3902000
3901000
3900000
3899000
419000
420000
421000
422000
423000
424000
425000
426000
427000

Figure 8

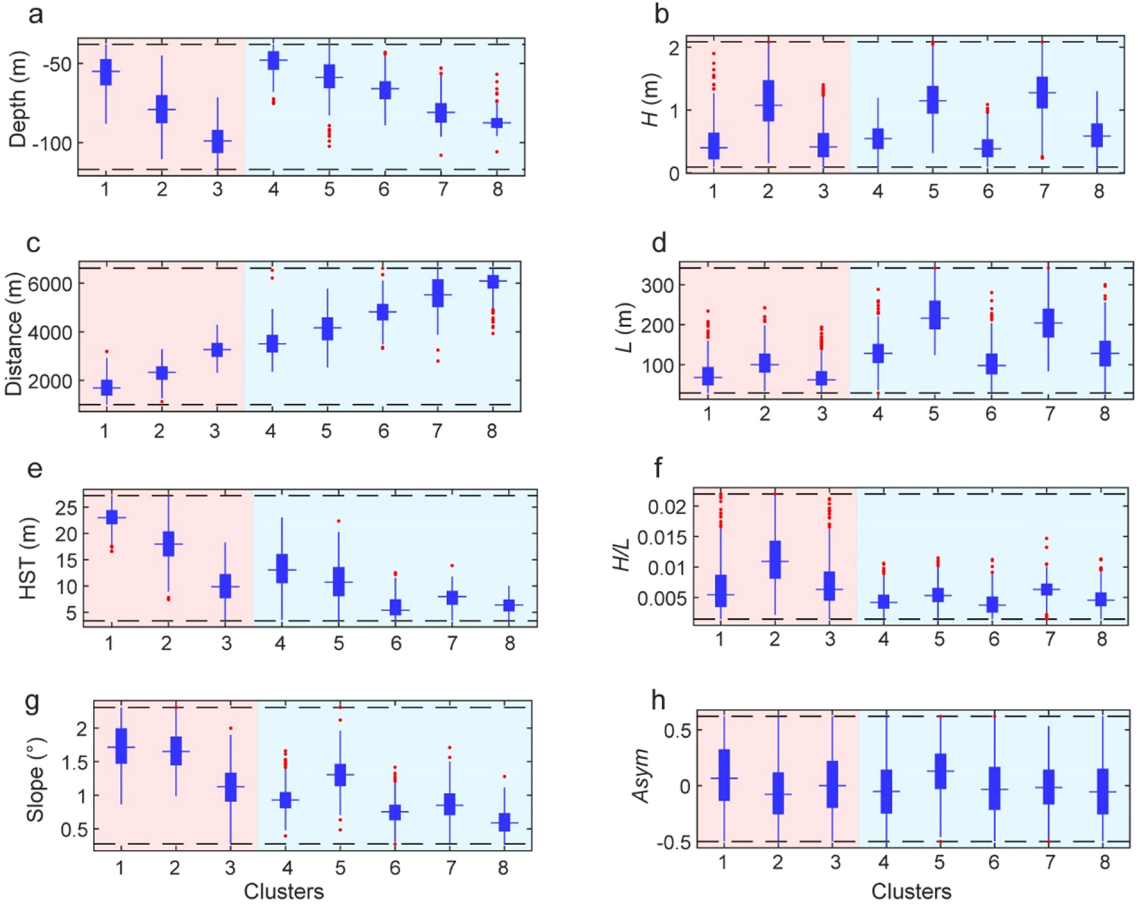
a
Depth (m)
-50
-100
1 2 3 4 5 6 7 8
b
H (m)
2
1
0
1 2 3 4 5 6 7 8
c
Distance (m)
6000
4000
2000
1 2 3 4 5 6 7 8
d
L (m)
300
200
100
1 2 3 4 5 6 7 8
e
HST (m)
25
20
15
10
5
1 2 3 4 5 6 7 8
f
H/L
0.02
0.015
0.01
0.005
1 2 3 4 5 6 7 8
g
Slope (°)
2
1.5
1
0.5
1 2 3 4 5 6 7 8
Clusters
h
Asym
0.5
0
-0.5
1 2 3 4 5 6 7 8
Clusters

Figure 9

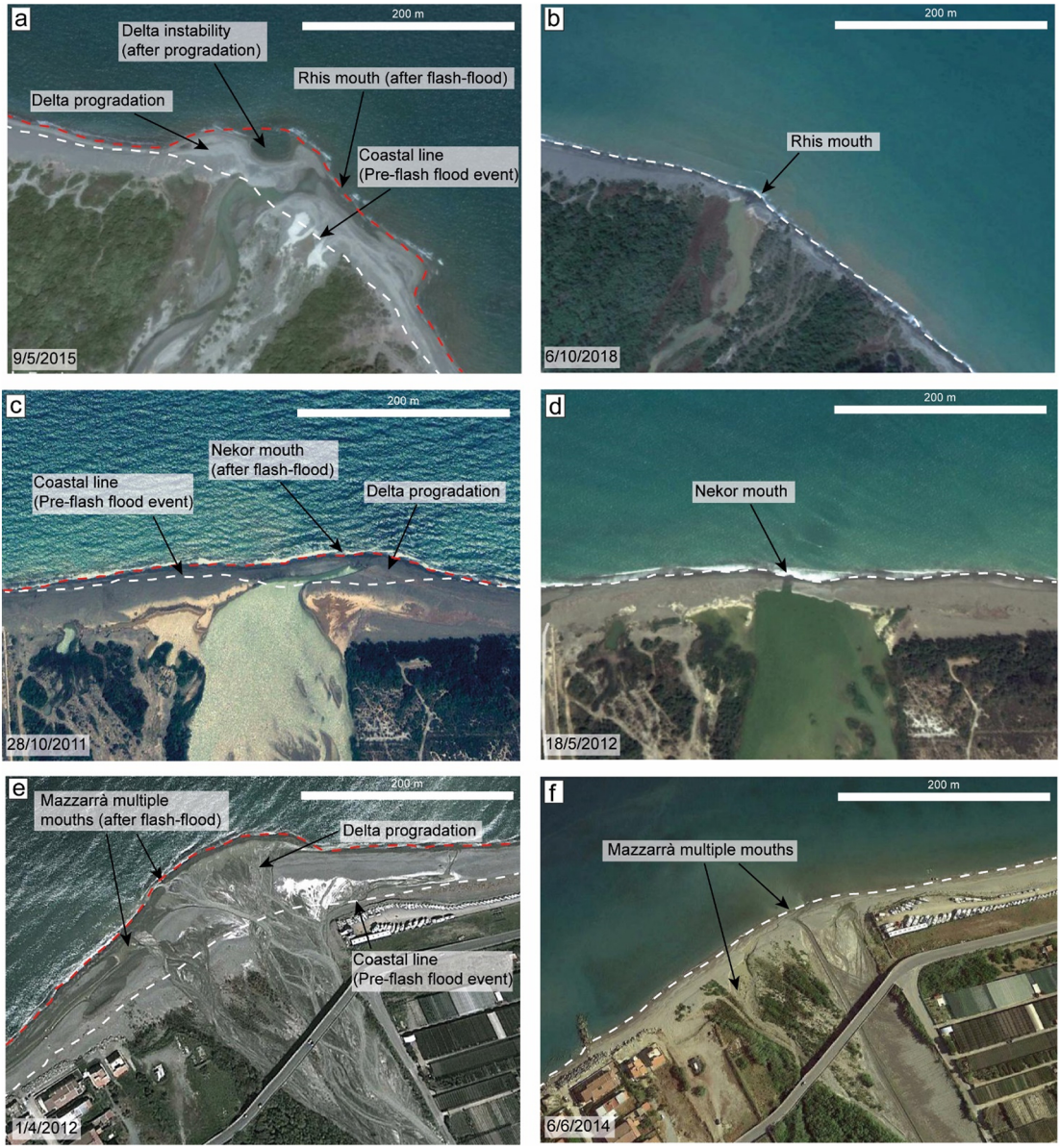
a
200 m
Delta instability
(after progradation)
Rhis mouth (after flash-flood)
Delta progradation
Coastal line
(Pre-flash flood event)
9/5/2015
b
200 m
Rhis mouth
6/10/2018
c
200 m
Nekor mouth
(after flash-flood)
Coastal line
(Pre-flash flood event)
Delta progradation
28/10/2011
d
200 m
Nekor mouth
18/5/2012
e
200 m
Mazzarrà multiple
mouths (after flash-flood)
Delta progradation
Coastal line
(Pre-flash flood event)
1/4/2012
f
200 m
Mazzarrà multiple mouths
6/6/2014

Figure 10

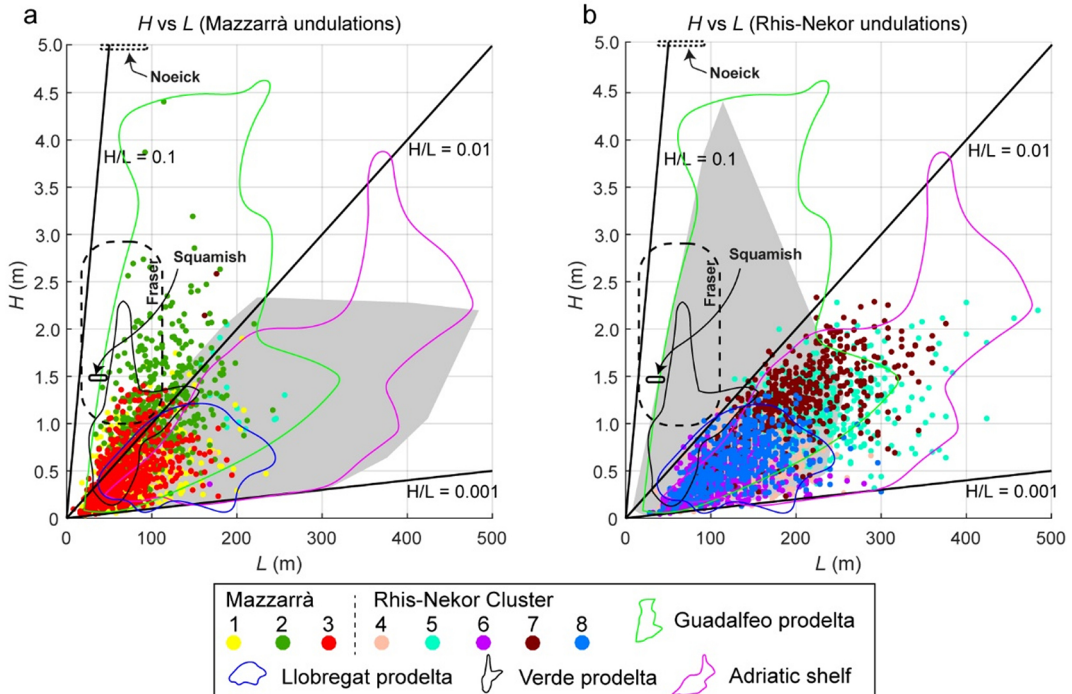
a
H vs L (Mazzarrà undulations)
b
H vs L (Rhis-Nekor undulations)
Noeick
H/L = 0.1
H/L = 0.01
H/L = 0.001
Squamish
Fraser
H (m)
L (m)
Mazzarrà
1 2 3
Rhis-Nekor Cluster
4 5 6 7 8
Guadalfeo prodelta
Llobregat prodelta
Verde prodelta
Adriatic shelf

Figure 11